Tree Physiology 39, 1646–1664 doi:10.1093/treephys/tpz078



Research paper

The stability enigma of hydraulic vulnerability curves: addressing the link between hydraulic conductivity and drought-induced embolism

Niels J.F. De Baerdemaeker ^{1,6}, Keerthika Nirmani Ranathunga Arachchige², Jana Zinkernagel³, Jan Van den Bulcke⁴, Joris Van Acker⁴, H. Jochen Schenk⁵ and Kathy Steppe ^{1,6}

¹Laboratory of Plant Ecology, Department of Plants and Crops, Faculty of Bioscience Engineering, Ghent University, Coupure Links 653, B-9000 Ghent, Belgium; ²Research Group Soil Genesis, Department of Environment, Faculty of Bioscience Engineering, Ghent University, Coupure Links 653, B-9000 Ghent, Belgium; ³Department of Vegetable Crops, Hochschule Geisenheim University, 65366 Geisenheim, Germany; ⁴UGCT—Laboratory of Wood Technology, Department of Environment, Faculty of Bioscience Engineering, Ghent University, Coupure Links 653, B-9000 Ghent, Belgium; ⁵Plants and H₂O Laboratory, Department of Biological Science, California State University Fullerton, PO Box 6850, Fullerton, CA 92834-6850, USA; ⁶Corresponding authors N.J.F. De Baerdemaeker (niels.debaerdemaeker@UGent.be); K. Steppe (kathy.steppe@UGent.be) ⑤orcid.org/0000-0001-6764-5784; ⑥orcid.org/0000-0001-6252-0704

Received October 3, 2018; accepted June 13, 2019; handling Editor Roberto Tognetti

Maintaining xylem water transport under drought is vital for plants, but xylem failure does occur when drought-induced embolisms form and progressively spread through the xylem. The hydraulic method is widely considered the gold standard to quantify drought-induced xylem embolism. The method determines hydraulic conductivity (K_h) in cut branch samples, dehydrated to specific drought levels, by pushing water through them. The technique is widely considered for its reliable K_h measurements, but there is some uncertainty in the literature over how to define stable K_h and how that relates to the degree of xylem embolism formation. Therefore, the most common setup for this method was extended to measure four parameters: (i) inlet K_h , (ii) outlet K_h , (iii) radial flow from xylem to surrounding living tissue and (iv) the pressure difference across the sample. From a strictly theoretical viewpoint, hydraulic steady state, where inflow equals outflow and radial flow is zero, will result in stable K_h . Application of the setup to Malus domestica Borkh. branches showed that achieving hydraulic steady state takes considerable time (up to 300 min) and that time to reach steady state increased with declining xylem water potentials. During each experimental run, K_h and xylem water potentials dynamically increased, which was supported by X-ray computed microtomography visualizations of embolism refilling under both high- (8 kPa) and low-pressure (2 kPa) heads. Supplying pressurized water can hence cause artificial refilling of vessels, which makes it difficult to achieve a truly stable K_h in partially embolized xylem.

Keywords: acoustic emissions, drought stress, hydraulic method, Malus domestica Borkh., X-ray computed microtomography.

Introduction

Vascular water transport has been referred to as the 'backbone of plant physiology' (Brodribb 2009) and is vital for plant functioning. It consists of two interconnected pathways: (i) the phloem, which distributes sugars throughout the plant, fueling

cell maintenance and growth (Van Bel 2003, Sala et al. 2012, Hubeau and Steppe 2015, Steppe et al. 2015) and (ii) the xylem, responsible for dynamic upward transport of water and nutrients (Tyree and Zimmermann 2002, Venturas et al. 2017), sometimes over more than 100 m to the canopy (Ryan et al. 2006, Kim et al. 2014). Both pathways are interconnected by

an intricate network of living cells in both xylem and phloem that can store large amounts of water (Sano et al. 2005, Pfautsch et al. 2015a). This storage function substantially contributes to the dynamic transport of water and is categorized into three components: (i) capillary water, (ii) water released from elastic living cells and (iii) water released from embolism formation (Tyree and Yang 1990, Tyree and Zimmermann 2002, Hölttä et al. 2009, Scholz et al. 2011, Vergeynst et al. 2015a, Pfautsch et al. 2015b, Steppe 2018).

Xylem can be described as a chain of continuous water columns, passively transporting water upward via cohesiontension forces (Dixon and Joly 1895). This transport mechanism is formulated as the widely accepted cohesion-tension theory. Though this transportation method does not require energy from the plant, it comes with the disadvantage of being metastable, as it is subjected to tension, i.e., negative water potentials (ψ , MPa) (Steudle 2001, Cochard et al. 2013). Increasing tension can potentially induce a phase transition of liquid water to vapor (Mayr et al. 2014), entry of air bubbles through cell wall pores (Zimmermann 1983) or expansion of preexisting gas nanobubbles in the sap (Schenk et al. 2015), all of which can result in a breakage of the continuous water columns and thus formation of embolisms (Tyree and Zimmermann 2002). If left unchecked, progressing drought stress and embolism can lead to plant mortality, and hence limit biomass production (Brodribb et al. 2010, Melcher et al. 2012).

Quantifying a plant species' vulnerability to drought-induced embolism and the resulting decrease in xylem hydraulic conductivity is becoming increasingly more important as climate change increases the frequency, duration and severity of drought and heat stress events (Allen et al. 2010). For this purpose, a wide variety of methods have been developed, differing in the ways embolism is induced and how its effects are measured (Cochard et al. 2013). Despite the existence of different techniques, the gold standard remains the hydraulic method first introduced by Sperry et al. (1988a) and later modified in various ways in many studies (Espino and Schenk 2011), such as using more rigid tubing to minimize tubing volume changes and additional calculation steps to account for background flow rate (Hacke et al. 2000, Torres-Ruiz et al. 2012). In this method, embolism in a plant sample is induced by bench-top dehydration and quantified by measuring loss in hydraulic conductivity. The original technique uses a hydraulic system where an aqueous solution is sent via a small positive pressure head (range 1-8 kPa) through a cut branch sample, while the resulting flow rate at the outlet side is measured by a precision balance (Sperry et al. 1988a), but a wide variety of solutions and pressure heads (up to 70 kPa) have since then been utilized in various studies (Espino and Schenk 2011). In a different approach, only the inlet flow is measured using a flow meter (Cochard et al. 2000).

The Van den Honert (1948) concept describes that stationary flow of water is determined by the water potential gradient

between two points in the hydraulic pathway and the resistance across it (Tyree and Ewers 1991). Sperry et al. (1988a) first used this pressure–flow relationship to translate mass flow rate to K_h by determining the pressure difference over the cut sample. The technique is repeated on samples with different degrees of embolism formation in order to quantify loss in K_h , which is then rescaled to percentage loss in conductivity (PLC, %), by calculating maximum hydraulic conductivity ($K_{h,max}$) of the respective samples, and dividing the two quantities (Eq. (1)):

$$PLC = \left(1 - \frac{K_h}{K_{h,max}}\right) \times 100 \tag{1}$$

If the water potential of the cut branch samples is determined, then a vulnerability curve (VC) can be constructed, relating percentage loss in K_h to xylem tension (Sperry et al. 1988c). The universal index P_{50} (MPa), representing xylem tension at which 50% loss in K_h occurs, can be derived from the VC and is widely used to classify the degree of vulnerability to drought-induced embolism in plants (Choat et al. 2012, Melcher et al. 2012).

Following the method described by Sperry et al. (1988a), correct assessment of K_h is based on a deviating trend in running mean (RM), and this approach implies a stable condition in outflow (Melcher et al. 2012). The reported timespan to reach this stability in K_h is typically within the first 30 min of measurement (Cochard 2006) and varies depending on sample characteristics and examined species: Espino and Schenk (2011) reached stability within the first 5 min in fully hydrated samples, Nardini et al. (2012) within 20-40 min, and 10-15 min was recorded in Trifilò et al. (2014). Variation in timespans makes it difficult to reproduce hydraulic experiments, especially when different criteria are used to define stability in K_h , and reproducibility is even harder when timespans are not mentioned (e.g., Torres-Ruiz et al. 2012, Beikircher et al. 2013) or when stability criteria are not specifically described (e.g., Hacke et al. 2000, Hacke and Sperry 2003, Jacobsen et al. 2005).

Recently, it has been shown that hydraulic stability is not reached within timespans typically used in hydraulic experiments. Simultaneous measurements of inflow and outflow through herbaceous stems of asparagus (Asparagus officinalis L.) demonstrated that much of the water supplied to a drying stem moved radially into stem tissue, with inflow exceeding outflow by $5.89 \pm 2.03 \ 10^{-6} \ m^2 \ MPa^{-1} \ s^{-1}$ at a stem water potential of $-0.5 \ MPa$ (Figure 1) and further increasing to $3.14 \pm 7.51 \ 10^{-5} \ m^2 \ MPa^{-1} \ s^{-1}$ at water potentials below $-2 \ MPa$ (Zinkernagel and Mayer 2018). It is likely that this radial flow into stem tissues will affect hydraulic conductivity even after steady-state is reached and even could contribute to refilling embolized vessels.

Studies also differ in the pressure head applied to samples during conductivity measures. Low-pressure heads are typically

Table 1. Applied pressure heads in different studies to measure hydraulic conductivity (K_h) of various plant species.

Pressure head (kPa)	Plant species/plant group	Study	
6–7	A. saccharum Marshall	Sperry et al. (1988a)	
3	Shrub species from the Great Basin, Utah	Hacke et al. (2000)	
6	Mediterranean woody species	Martinez-Vilalta et al. (2002)	
4–6	Diffuse-porous and conifer species	Li et al. (2008)	
2–3	Ring-porous species	Li et al. (2008)	
1.6; 7	Vitis vinifera L.	Choat et al. (2010)	
2.5; 5.0; 7.5; 10	A. officinalis L.	Zinkernagel et al. (2011)	
1–2	V. vinifera L.	Jacobsen and Pratt (2012)	
8	Acer var.	Nardini et al. (2012)	
4–5.5	Olea europaea L.	Torres-Ruiz et al. (2012)	
4	M. domestica Borkh.	Beikircher et al. (2013)	
6	Quercus ilex L.	Martin-St Paul et al. (2014)	
8	Laurus nobilis L. and O. europaea L.	Trifilò et al. (2014)	
8–8.5	Humulus lupulus L., V. vinifera L. and Clematis vitalba L.	Balaz et al. (2016)	
2–4	Chaparral shrub species	Jacobsen et al. (2016)	
1.5–2	Chaparral shrub species	Venturas et al. (2016)	

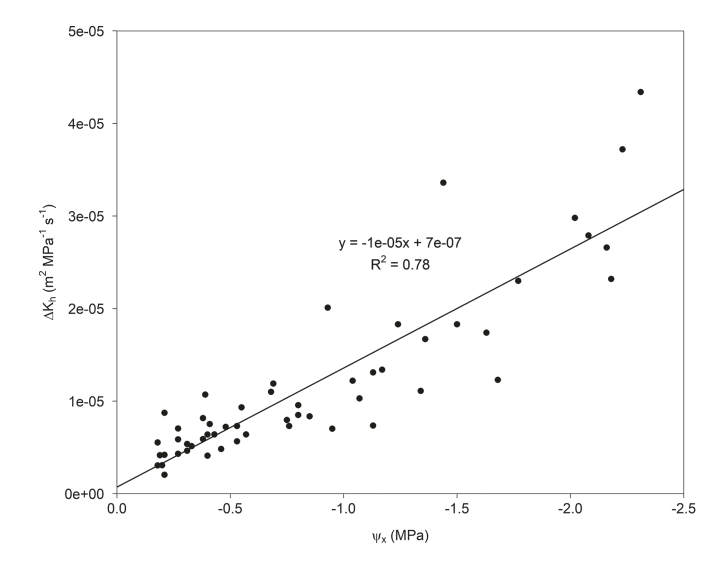


Figure 1. Influence of xylem water potential (ψ_x , MPa) on the difference in hydraulic conductivity (ΔK_h , m² MPa¹ s⁻¹) between inlet and outlet of asparagus shoot segments (modified with permission from Zinkernagel and Mayer (2018)).

applied, as they are assumed to avoid embolism refilling during conductivity measurements (Kolb et al. 1996, Sperry et al. 1988a, Melcher et al. 2012). However, even within the range of low-pressure heads, examined species and research objectives make it difficult to standardize pressure heads (Table 1). The maximum applicable pressure head that is expected to avoid embolism displacement for a given species can be estimated from vessel diameter as $P = 2\sigma/r_{\rm V}$, with σ representing the surface tension of water at 20 °C (0.0728 N m⁻¹) and $r_{\rm V}$ the radius of the widest vessel (Van leperen et al. 2000, Melcher et al. 2012), but that method should be further investigated in light of recent discoveries of low surface tension in xylem (Christensen-Dalsgaard et al. 2011, Schenk et al. 2018).

Despite the advances in plant hydraulic research, neither physiological nor theoretical nor physical explanations are available to justify a particular timespan for reaching stability in K_h and which pressure heads to use. By extending the original setup with additional measurements, our study aimed at quantifying water flow dynamics through cut branch samples of *Malus* domestica Borkh. when used in the hydraulic method to explain some of the reported uncertainties. Without questioning the reliability of the method in measuring K_h , it is however important to formulate the right criterion to determine which of the measured K_h values is best suited to reflect the degree of droughtinduced embolism formation, and thus for construction of the hydraulic VC. Following up on two previous studies in which both inlet flow and outlet flow were determined (Espino and Schenk 2011, Zinkernagel and Mayer 2018), we measured (i) inlet K_h with a flow meter, (ii) outlet flow with a precision balance, and added (iii) measurement of diameter change as proxy of radial flow between xylem and surrounding living tissue with a linear variable displacement transducer (LVDT) and (iv) the pressure difference across the sample with pressure sensors. Stability in conductivity was defined following fluid dynamics theory; more specifically, hydraulic steady state is reached when inflow equals outflow and radial flow becomes zero. To assess the effect of pressure heads on conductivity measurements, a low (2 kPa) and high (8 kPa) pressure head were applied in the setup. In addition, the impact of the hydraulic method on xylem tension was assessed, and X-ray computed microtomography (µCT) was used to verify the degree of xylem embolism in response to drying, flushing and hydraulic measurements with different pressure heads. Finally, acoustic emissions (AE) were measured on dehydrating M. domestica Borkh. branches to construct acoustic VCs and assess whether these can be reliable substitutes for constructing VCs without the risk of hydraulic artifacts.

Materials and methods

Plant material

Malus domestica Borkh. branches for hydraulic conductivity and μCT measurements were collected during August and September 2016, while AE measurements were carried out in August 2017 (day of year (DOY) 214 until DOY 215). Comparison between AE and hydraulic method over consecutive years is justified because the trees were grown under a moist and temperate climate in sand-lime soil at the Faculty of Bioscience Engineering, Ghent University, Belgium $(51^\circ03'10.3''N)$ latitude; $3^\circ42'32.3''E$ longitude). The trees had an average diameter at breast-height of 17.2 ± 1.7 cm and an average height of 3.6 ± 0.7 m. They were around 15 years old and were pruned every 2–3 years, and aside from being rainfed, no additional watering was supplied.

Maximum vessel length

Maximum vessel length was determined by connecting the proximal end of cut branches to a compressed air tank via flexible tubing (Zimmermann and Jeje 1981, Ewers and Fisher 1989). Air was then pressurized to 100 kPa and sent through the branch, with the apical end submerged in water. The branch was gradually cut back until a steady stream of bubbles originated from one xylem vessel element. Branch length was measured, which represented the length of the longest vessel. The maximum vessel length of M. domestica Borkh. was on average equal to 58.9 ± 6.4 cm (n = 10).

Sampling procedure for the hydraulic, μ CT and AE method

Branches for the hydraulic, µCT and AE method were cut underwater before sunrise to achieve full hydration of functional vessels see (Figure 8A; De Baerdemaeker et al. 2017). To ensure that xylem tension at the time of cutting was near zero to avoid cutting artifacts (Cochard et al. 2013, Wheeler et al. 2013), three alternate leaves near the apical end of the branch were covered in aluminum foil the day prior to measurement. Wrapping the leaves in aluminum foil allows leaf water potential to equilibrate with xylem tension by lowering stomata conductance and transpiration (Trifilò et al. 2014, De Baerdemaeker et al. 2017). After branch excision, xylem water potential (ψ_x , MPa) was determined with a pressure chamber (Model 1000, PMS Instrument Company, Albany, OR, USA; Scholander et al. 1965) and found to be 0 MPa for all cut branches. Hydraulic branches were on average 113 \pm 7 cm long (n = 18), μ CT branches 115 \pm 7 cm (n = 5) and AE branches 114 ± 8 cm (n = 4). The length of the study branches was around twice the maximum vessel length to avoid artificially created embolisms from the cutting procedure (Melcher et al. 2012, Cochard et al. 2013, Torres-Ruiz et al. 2015). The cut end was then submerged in a water-filled bucket, and the branches were covered with a black polyethylene bag during

transportation to the lab, which was about 2 min removed from the sampling site.

Sample preparation hydraulic method

A 15 cm section was marked in the middle of the branch, with an average diameter of 7.56 \pm 0.07 mm (n = 18). This 15 cm section was chosen to allow to a certain extent comparison with the 15 cm long samples used in the original hydraulic method on Acer saccharum Marshall (Sperry et al. 1988a). The 15 cm length is also the most common length for xylem vulnerability studies using the centrifuge method (Alder et al. 1997). Study branches were subjected to different bench-top dehydration periods: 0, 2, 4, 6, 8, 10, 12, 14 and 16 h. Two additional steps were executed prior to dehydration: (i) removal under water of all but one leaf in the marked 15 cm section. Wounds were covered with superglue to limit leakage and dehydration, potentially disrupting conductivity measurements. (ii) Covering three leaves close to the 15 cm section with aluminum foil, to determine xylem tension at the end of each bench-top dehydration period, while the remaining leaves were left exposed to speed-up the dehydration process. Following each dehydration period, branches were gradually shortened underwater up to the 15 cm section, which allowed sufficient time to relax the tension and avoid cutting artifacts (Cochard et al. 2013, Wheeler et al. 2013). Additional care was taken to keep the remaining leaf above the water surface during cutting. The section was then wiped, and the remaining leaf was covered in aluminum foil (Figure 21, Figure S1E1 available as Supplementary Data at Tree Physiology Online). From both ends of the sample, 0.5 cm of bark was removed with a sharp knife to ensure that water directly entered the xylem vessels. To avoid the pinching effect of the garden shears used to shorten the branches, both ends were cut transversally with a sharp knife to reopen the vessels. Parafilm was wrapped around the bark at both ends to allow a smooth fit with the silicone connection tubes of the hydraulic conductivity apparatus.

Hydraulic conductivity apparatus

The hydraulic conductivity apparatus was built to mimic the original setup described by Sperry et al. (1988a), where K_h is obtained by measuring the flow rate at the outlet side via an electronic precision balance (Figure 2L, Figure S1F1 available as Supplementary Data at *Tree Physiology* Online). To unravel water flow dynamics in the study samples during K_h measurements, the apparatus was enhanced (Figure 2, Figure S1 available as Supplementary Data at *Tree Physiology* Online), allowing for a complete assessment of the hydraulic method, by expanding it with a flow meter (Liqui-Flow with 0–20 g h⁻¹ range and 0.05 g h⁻¹ accuracy, Bronckhorst (High Tech), Montigny les Cormeilles, France) at the inlet side (Figure 2D, Figure S1C available as Supplementary Data at *Tree Physiology* Online), a LVDT (LVDT, DF/5.0, Solartron Mobrey, Brussels,

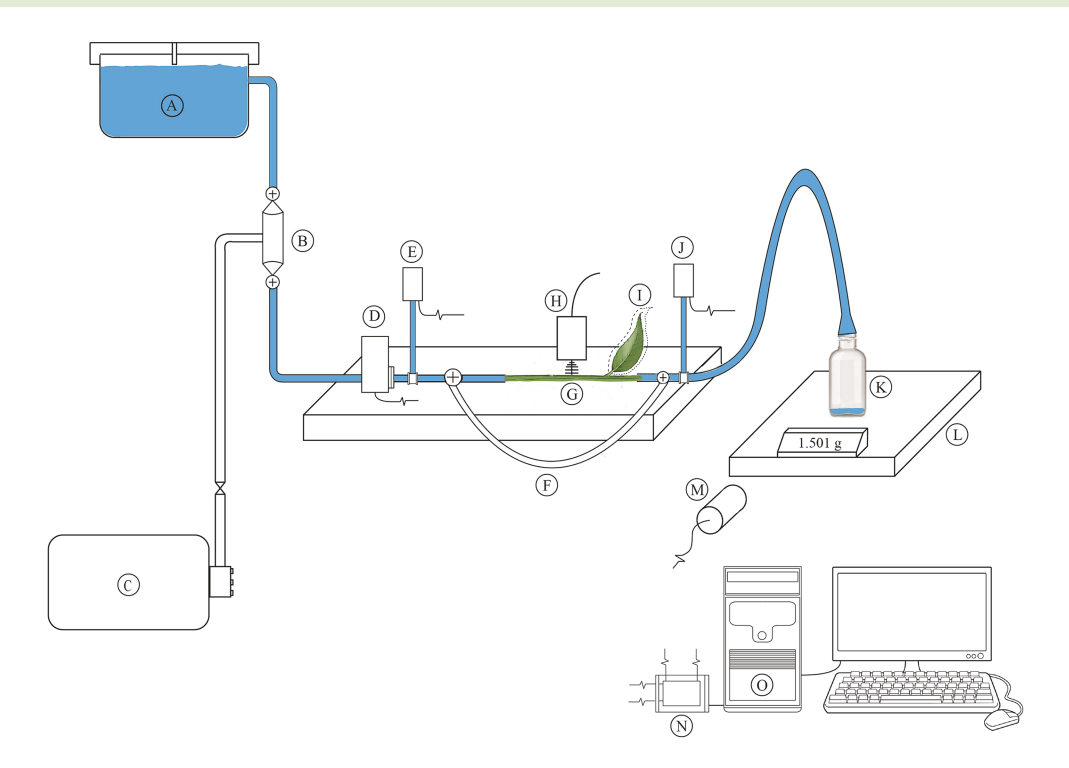


Figure 2. Schematic of the modified hydraulic conductivity apparatus used for hydraulic conductivity measurements: (A) reservoir with Volvic water to induce required pressure head; (B) Liqui-Cel mini module degasser; (C) vacuum pump; (D) Liqui-Flow flow meter; (E) and (J) Vegabar14 pressure sensor; (F) bypass tube; (G) cut *M. domestica* Borkh. branch sample; (H) LVDT; (I) aluminum covered leaf; (K) receptacle; (L) electronic precision balance; (M) Guardo Action Cam +; (N) Campbell scientific CR1000 data logger; and (O) computer.

Belgium) perpendicular to the sample surface (Figure 2H, Figure S1E2 available as Supplementary Data at Tree Physiology Online) and two pressure sensors (Vegabar14 with 0-10 kPa range and 0.01 kPa accuracy, Schiltach, Germany) at both ends of the study sample (Figure 2E-J, Figure S1D available as Supplementary Data at Tree Physiology Online). Two different pressure heads (2 and 8 kPa) were applied to assess possible embolism refilling. The pressure heads were set by changing the height of the hydraulic head, which was a reservoir with a broad surface to ensure that the pressure head remained fixed at 2 or 8 kPa during the course of the conductivity experiment (Figure 2A, Figure S1A available as Supplementary Data at Tree Physiology Online). The supplied solution to the reservoir was commercially bottled mineral Volvic water (Volvic natural mineral water, Danone waters group, France; pH = 7.2, 8.0 mg I^{-1} Na, 10.4 mg I^{-1} Ca, 6.0 mg I^{-1} Mg, 4.0 mg I^{-1} SO₄), because it closely resembles the ion composition of xylem sap (S. Jansen, personal communication). Micropur tablets (Micropur Forte MF 1T, Katadyn Inc., Kemptthal, Switzerland) were added to the Volvic solution to prevent formation of bacteria and viruses. A lid prevented evaporation and contamination of the solution, but was placed loosely onto the reservoir to avoid pressure buildup in the system. A mini-degassing module (Liqui-Cel mini module G543, Membrana, Charlotte, NC, USA), connected to a vacuum pump (MVP055-3, Pfeiffer Vacuum, Assiar, Germany), was installed between the reservoir and the sample

to remove air bubbles from the solution in order to avoid artificial embolism formation (Figure 2B and C, Figure S1B available as Supplementary Data at Tree Physiology Online; Espino and Schenk 2011). No filter was used. The average particle size in the solution was 84.4 \pm 40.7 nm, and 95% of the particles had a size lower than what could be removed by a standard 200 nm filter (Figure S2 available as Supplementary Data at *Tree Physiology* Online). The size distribution and concentration of nanoparticles in Volvic water with Micropur tablet were determined by light scattering-based single particle tracking using a NanoSight LM10-HS instrument (Malvern Instruments Ltd, Malvern, UK) equipped with a 488 nm laser. Movies of 60 s were recorded while the data were analyzed with the NTA Analytical Software version 3.2 (Malvern Instruments Ltd, Malvern, UK). Branch samples were installed in a custom-built holder (Figure S1E available as Supplementary Data at Tree Physiology Online), which ensured a stable installation of both the LVDT and sample. The silicone tubes that connect the sample to the apparatus were manually filled with Volvic water via a syringe. Care was taken when connecting the sample via plastic clamps to these silicone tubes to avoid formation of air bubbles. Tissue paper was put underneath the connections to check for leakages. In case of leaks, sample measurement was stopped, discarded and repeated. A bypass tube was installed to flush the hydraulic apparatus before and after each experiment (Figure 2F, Figure S1E3 available as Supplementary

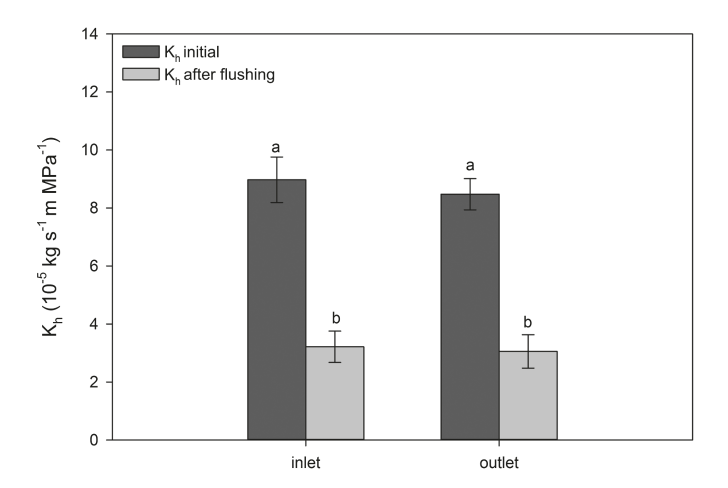


Figure 3. Difference between average hydraulic conductivity (K_h , 10^{-5} kg s⁻¹ m MPa⁻¹) of freshly cut M. domestica Borkh. samples (dark gray, K_h initial), and average K_h of flushed samples (light gray, K_h after flushing) at both the inlet and outlet sides (n = 5) with their standard error (1 SE). Significant differences are indicated with different letters (P < 0.05). Freshly cut K_h was significantly higher than flushed K_h at both the inlet and outlet sides (P = 0.00031 and 0.00013, respectively).

Data at *Tree Physiology* Online) to remove air bubbles and contaminations. Flushing lasted for 10 min by connecting the apparatus to an inox pressure case (pressure case RVS 24L spray-matic, Air Compact, Gentbrugge, Belgium), which was filled with Volvic water and pressurized to 100 kPa (Figure S3A available as Supplementary Data at *Tree Physiology* Online). A receptacle was placed at the end of the apparatus to catch the outflowing solution (Figure 2K, Figure S1F2 available as Supplementary Data at *Tree Physiology* Online). The opening was covered with Parafilm to avoid evaporation, but a small incision was made to avoid pressure buildup in the system. The precision balance with receptacle, Parafilm cover and water-filled tubing was tared before the start of each K_h measurement to only account for the outflow effect.

Data were collected every 5 s and averaged over 1 min for the flow meter, pressure sensors and LVDT, and were measured as millivolt (mV) signals via a data acquisition system (CR1000, Campbell Scientific, Logan, UT, USA), which was connected to a computer (Figure 2N and O, Figure S1 available as Supplementary Data at *Tree Physiology* Online). Values were monitored live with the LOGGERNET software (LOGGERNET 4.5, Campbell Scientific). The precision balance could not be logged and therefore photos of the display were taken every minute with a camera (Guardo Action Cam +, TE-GROUP nv, Kapellen, Belgium; Figure 2M, Figure S1F3 available as Supplementary Data at *Tree Physiology* Online).

Hydraulic conductivity

Sample measurements typically lasted longer than half a day to ensure that \mathcal{K}_h based on hydraulic steady state could be

quantified. Hydraulic steady state was determined using two approaches: (i) stability in K_h , which refers to the point when K_h at the inlet side approximates K_h at the outlet side within a threshold range of 6 \pm 1 10^{-8} kg s⁻¹ m MPa⁻¹ or the difference between both becomes minimal. This assumption is justified, because the difference in inlet (P_{in}) and outlet pressure (P_{out}) remained constant during the course of conductivity measurements (Figure 4). Volvic water will only flow through the xylem in that case. (ii) The second approach used stability in diameter change (Δd , mm), which refers to the point where the change in branch diameter flattens out. Then, water is no longer directed to living cells to replenish them and radial flow will be minimal, no longer influencing xylem hydraulic conductivity. K_h values were also recorded at the start of each conductivity experiment or using a deviation in RM of the outflow (Sperry et al. 1988a). Calculation of RMs was based on the previous five 1-min conductivity readings, and they were plotted against time to determine at which point the trend in RM deviated from a previous decreasing/increasing trend.

Raw data extracted from the data logger (mV) were converted to diameter change (Δd , mm) for LVDT, inflow ($F_{\rm in}$, g h⁻¹) for flow sensor, and inlet ($P_{\rm in}$, MPa) and outlet pressure ($P_{\rm out}$, MPa) for pressure sensors, by using their respective calibration equations. The camera time was extracted from metadata by using Phyton 2.7.13 software. For each specific time interval (t, h) derived from metadata, weight readings of the balance (W, g) were entered manually and converted to outflow data ($F_{\rm out}$, g h⁻¹; Eq. (2)):

$$F_{\text{out}} = \frac{W_{i+1} - W_i}{t_{i+1} - t_i}$$
 (2)

The offset between camera and logger time was fixed by linearly interpolating $F_{\rm out}$ over fixed 1 min time intervals using the PhytoSim software package (PhytoSim 2.1, Phyto-IT, Gent, Belgium). Inlet ($K_{\rm h,in}$, 10^{-5} kg s⁻¹ m MPa⁻¹; Eq. (3)) and outlet ($K_{\rm h,out}$, 10^{-5} kg s⁻¹ m MPa⁻¹; Eq. (4)) hydraulic conductivities were calculated by incorporating the length of the sample ($L_{\rm sample}=0.15$ m) and the pressure difference ($P_{\rm in}-P_{\rm out}$, MPa) over the sample. By directly measuring the pressure drop over the sample, corrections for passive water uptake were not required (Torres-Ruiz et al. 2012):

$$K_{h,in} = \left(\frac{\frac{F_{in}}{1000 \times 3600} \times L_{sample}}{P_{in} - P_{out}}\right) \times 10^{5}$$
 (3)

$$K_{\text{h,out}} = \left(\frac{\frac{F_{\text{out}}}{1000 \times 3600} \times L_{\text{sample}}}{P_{\text{in}} - P_{\text{out}}}\right) \times 10^5 \tag{4}$$

Maximum hydraulic conductivity

Maximum hydraulic conductivity ($K_{h,max}$) was assessed after initial conductivity measurements (Cochard et al. 2013), by flushing the samples with degassed Volvic water for 1 h with 100 kPa of pressure (Figure S3 available as Supplementary

Data at Tree Physiology Online; Jacobsen et al. 2005). The flushing procedure seemed to work for refilling as air was removed from the sample (Figure S3B available as Supplementary Data at Tree Physiology Online), but flushed conductivity was almost three times lower than initial conductivity (Figure 3). Therefore, $K_{h,max}$ was calculated in an alternative way, by assuming that maximum hydraulic conductivity coincides with the conductivity value of freshly cut branches of well-irrigated plants before sunrise. $K_{h,max}$ was determined under both pressure heads at both the inlet and outlet side, calculated over a maximum timespan of 30 min (Cochard 2006) and chosen in accordance to hydraulic steady state between inflow and outflow. The average of obtained $K_{h,max}$ values for each pressure head and side (n = 5) was used for the remainder of the experiment to calculate PLC (Eq. (1)) and is referred to as $K_{h,max}$ from freshly cut branches.

Hydraulic VC

The hydraulic VC was obtained by plotting percentage loss of conductivity (PLC, %) against xylem water potential (ψ_x , MPa) for each consecutive bench-top dehydration period. Four types of hydraulic VCs were constructed for each of the two pressure heads: (i) hydraulic steady-state VC according to equal $K_{h,in}$ and $K_{h,out}$, (ii) hydraulic steady-state VC according to minimal or zero radial flow between xylem and surrounding living tissue—this was determined via a segmented regression on diameter change (Muggeo 2008), where the distinct breakpoint indicated a clear transition between fast and slower increase in diameter; (iii) VC based on a deviation in RM of the outflow (Sperry et al. 1988a); and (iv) VC constructed from the first measured conductivity values. To calculate the change in xylem water potential measured at the end of benchtop dehydration and at the end of the conductivity experiment, an average was made of two relationships: (i) a linear relation between continuous LVDT diameter change and the two ψ_{x} point measurements (Vergeynst et al. 2015a) and (ii) a linear relation between time and the two ψ_x point measurements. The VC x-axes could then be adjusted so that conductivity values matched with the prevailing steady-state xylem tension at that time.

Acoustic emission sample preparation and data registration

Four branches were sampled for AE measurements and transported to an experimental room, which was lit with an artificial green light during preparation steps to diminish photosynthesis and transpiration (De Baerdemaeker et al. 2017, Epila et al. 2017). Wet cloths were fixed against the cut end of the branches to avoid air entry, and branches were placed in custombuilt holders to ensure an unbiased link and an equal distance (8 cm) between the two sensor types (De Baerdemaeker et al. 2017, Epila et al. 2017). Broadband point-contact AE sensors (KRNBB-PC, KRN Services, Richland, WA, USA) mon-

itoring acoustic activity and dendrometers (DD-S, Ecomatik, Dachau, Germany) measuring xylem shrinkage were installed on a section of exposed xylem (1.5 \times 0.5 cm). The AE sensor was pressed against the xylem via a compression spring (D22050, Tevema, Amsterdam, The Netherlands) in a small PVC tube. A droplet of vacuum grease (High-Vacuum Grease, Dow Corning, Seneffe, Belgium) was added between the sensor tip and branch to ensure good acoustic contact, which was validated via the pencil lead break test (Tyree and Sperry 1989b, Vergeynst et al. 2015b). Petroleum jelly was applied between the dendrometer tip and xylem, to avoid evaporation from the exposed wound (Vergeynst et al. 2016). After installation, wet clothes were removed and normal light was turned on in order to start the bench-top dehydration experiment.

Readings from dendrometers were registered every minute via custom-built acquisition boards. The AE signals were amplified by 35.6 decibels (dB) (AMP-1BB-J, KRN Services) and waveforms of 7168 samples length were acquired at 10 MHz sample rate. The signals were collected using two 2-channel PCI boards and redirected to the software program AEwin (PCI-2, AEwin E4.70, Mistras Group BV, Schiedam, The Netherlands). A 20-1000 kHz electronic band pass filter was applied and only waveforms above the noise level of 28 dB were retained (Vergeynst et al. 2016). To determine the decrease in xylem water potential of AE branches, no more than three leaves were wrapped in aluminum foil at any given time, while the remainder were left exposed to ensure a similar dehydration time conform to hydraulic branches. Water potential readings were done every 20 min, providing a sufficient 1-h timespan for a newly wrapped leaf to come in equilibrium with branch xylem. Both during leaf removal and wrapping, AE detection was interrupted to avoid noise (De Baerdemaeker et al. 2017, Epila et al. 2017).

Acoustic VC

The obtained AE signals were used to construct an acoustic VC (VCAE) (Mayr and Rosner 2011, Vergeynst et al. 2015a, De Baerdemaeker et al. 2017). The AE signals were cumulated over the measurement period from which the first derivative was calculated to construct an AE activity curve. The endpoint of the VC was determined as the point at which the decrease in AE activity, following the AE activity peak, decreased most strongly. From a mathematical point of view this corresponds to the local maximum of the third derivative (Vergeynst et al. 2016). Four branches were bench-top dried for 24 h, providing sufficient time to reach complete dehydration, as was validated by the µCT image of a 16-h-dehydrated M. domestica Borkh. branch, illustrating near full embolism formation (see Figure 10). The AE activity was calculated using a 5-min time interval, whereas the third derivative was determined using a 12-h time interval, based on the time scale at which the AE peak occurred (Vergeynst et al. 2016). The continuous x-axis of the acoustic VC (VC_{AE}) was obtained by establishing a segmented linear relation between xylem diameter shrinkage ($\Delta d/d_i$, μm mm⁻¹) and discrete measurements of ψ_x (De Baerdemaeker et al. 2017).

X-ray computed microtomography

To unravel water flow dynamics in the study samples during conductivity measurements, different aspects were investigated via µCT: (i) native embolism of freshly cut branches, (ii) the effect of flushing, (iii) the duration of the bench-top dehydration period to reach full embolism formation and (iv) the possibility of low-pressure heads refilling embolized vessels. Apple samples 15 cm long with a diameter similar to the sections used in the hydraulic method were scanned at the Nanowood CT facility (UGCT, Centre for X-Ray Tomography, Laboratory of Wood Technology, Faculty of Bioscience Engineering, Ghent University, Ghent, Belgium) (Dierick et al. 2014). Samples were fixed into a small Terostat-filled bottle (Terostat-IX, Teroson, Henkel, Düsseldorf, Germany) and centered via screws, with the open ends of the sample covered with Terostat to halter dehydration and air-entry (Figure S4 available as Supplementary Data at Tree Physiology Online). The targeted scanning point was taken \sim 5 cm below the top end and was marked with tape in the event scanning needed to be executed at the same height (for instance, a sample was first dehydrated and scanned, after which the same sample was installed in the hydraulic conductivity apparatus, and re-scanned to investigate the effect of a low-pressure head). The sample was loaded onto the rotation platform of the Nanowood µCT-scanner (UGCT, Centre for X-Ray Tomography) (Figure S4 available as Supplementary Data at Tree Physiology Online). Samples were scanned for 32 min, and the resulting 3.5-mm high 3D volume was reconstructed from 2000 projections taken during the 360° rotation. Reconstructions were made with the Octopus reconstruction software package (Dierick et al. 2004, Vlassenbroeck et al. 2007) and resulted in an approximate voxel pitch of 5 µm. To quantitatively examine the effect of dehydration and refilling, the difference between embolized (black) and water-filled (gray) vessels on the μCT images was calculated via the image analysis software Fiji (Schindelin et al. 2012) and translated to percentage via the total amount of vessels derived from the anatomical wood section of the species (Figure S5 available as Supplementary Data at Tree Physiology Online). This calculation illustrated that 52% of the vessels were embolized on the 6-h-dehydrated µCT image and was thus taking as proxy for the μ CT P_{50} .

Statistics

Analysis of variance was performed to detect differences between average K_h of freshly cut and flushed branches (P < 0.05), with values validated for normality and homogeneity via Wilcoxon signed rank test and Levene test, respectively. The acoustic VC (VC_{AE}) was averaged over the four branches and fitted using the smooth spline function in the stats library in R

software (RStudio version 1.1.419—© 2009–2017 RStudio, Inc., Boston, MA, USA). Xylem water potential at which 50% of embolism-related AE occurs (AE $_{50}$, MPa) was directly derived from the VCAE (De Baerdemaeker et al. 2017). Hydraulic VCs were fitted via the fitplc R package in the stats library of R software (Duursma and Choat 2017). Two types of models were fitted to the data via the R package: (i) the reparameterized Weibull function of Ogle et al. (2009) and (ii) a sigmoidal model as postulated by Pammenter and Van der Willigen (1998). A Weibull fit was justified only for hydraulic steady state in K_h for 8 kPa pressure head, because a xylem water potential of 0 MPa coincided with 0% PLC. From the fitplc package, P_{50} values of hydraulic VCs were calculated as well (Duursma and Choat 2017). Figures were made with RStudio and SigmaPlot 13 graphing software package.

Results

Hydraulic method

Measurements of hydraulic conductivity and branch diameter dynamically changed with time when using the hydraulic method (Figure 4). Independent of the duration of bench-top dehydration, Kh first decreased, reaching a local minimum, followed by an increase toward an absolute maximum and a further decrease until the end of the experimental run. Inlet hydraulic conductivity ($K_{h,in}$) started consecutively higher than outlet hydraulic conductivity ($K_{h,out}$), after which the difference between both decreased. Hydraulic steady state in conductivity was reached when $K_{h,in}$ approximately equaled $K_{h,out}$ for the first time within a threshold range of $6 \pm 1 \cdot 10^{-8} \text{ kg s}^{-1} \text{ m MPa}^{-1}$ (Figure 4A–C) or the difference between both became minimal (Figure 4D-F). Overall, the timespan to reach hydraulic steady state increased with the duration of bench-top dehydration (Figure 4, Table 2). Maximum K_h of hydrated samples (0 h of dehydration, reflecting the hydrated condition of non-detached branches; Zinkernagel et al. (2011)) corresponded well with $K_{h,max}$ measured on freshly cut branches, but absolute values of K_h and corresponding maximum values per experimental run decreased when longer sample dehydration periods were used (Figure 4, Table 3). For both pressure heads, the difference between $P_{\rm in}$ and $P_{\rm out}$ remained constant during the experimental run, but increased with dehydration level, because of the increase in resistance in the hydraulic pathway (Figure 4). Diameter change (Δd , mm) or radial flow from xylem to surrounding living tissues was negligible in hydrated samples (0 h of dehydration) but became important and pronounced in all dehydrated samples (Figure 4). The timespan to reach hydraulic steady state in radial flow also increased with dehydration level for the 8 kPa pressure head, but was less clear for the 2 kPa pressure head (Table 2). Initial xylem water potentials (ψ_x , MPa), measured after each bench-top dehydration step and thus prior to the experimental run, became more negative

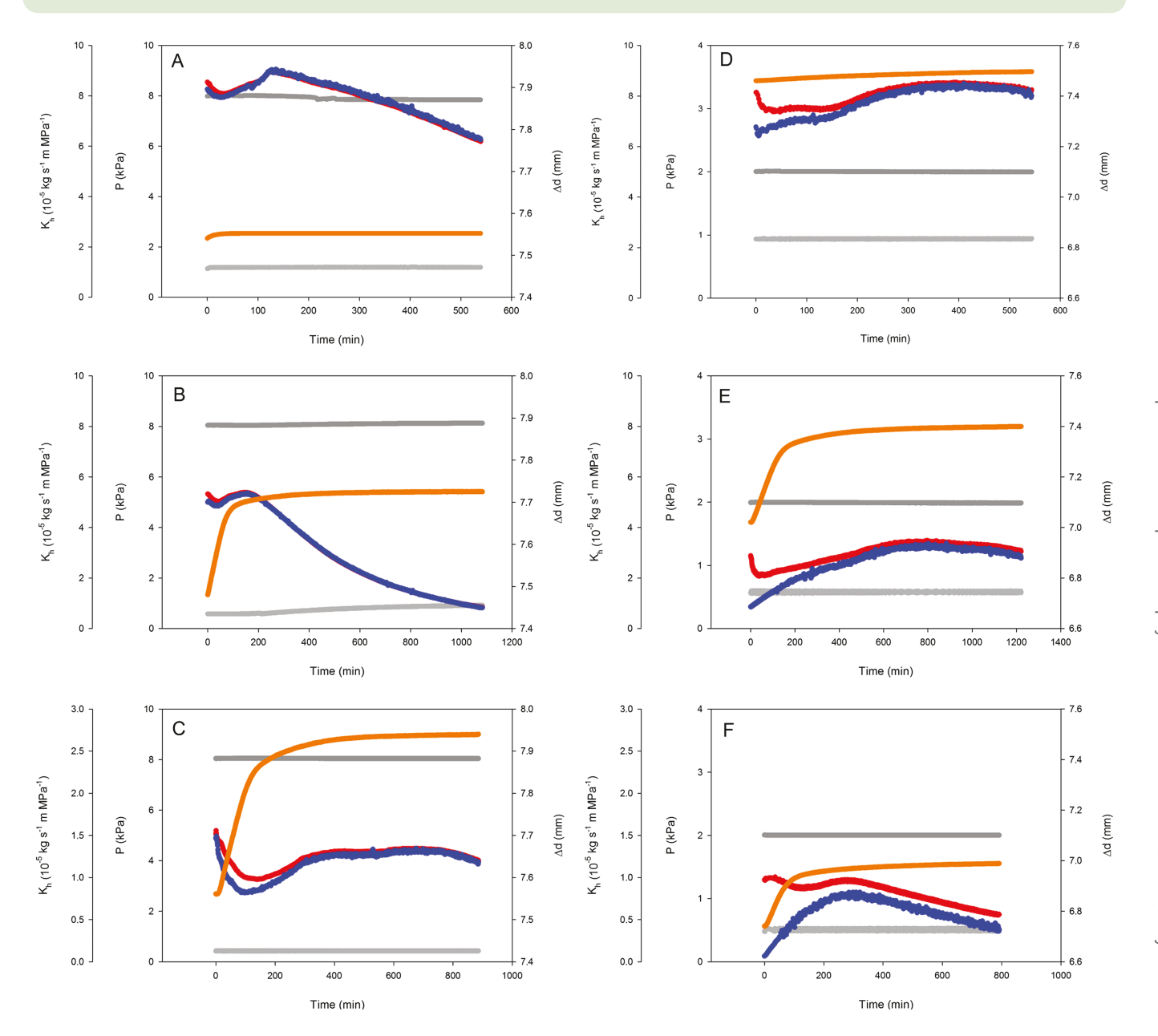


Figure 4. Change in inlet pressure (gray, P_{in} , kPa), outlet pressure (light gray, P_{out} , kPa), stem diameter or radial flow (orange, Δd , mm), inlet hydraulic conductivity (red, $K_{h,in}$, 10^{-5} kg s⁻¹ m MPa⁻¹) and outlet hydraulic conductivity (blue, $K_{h,out}$, 10^{-5} kg s⁻¹ m MPa⁻¹) of M. domestica Borkh. samples for two different pressure heads (8 kPa: A–C; 2 kPa: D–F) and for three different bench-top dehydration periods (0 h: A, D; 6 h: B, E; 12 h: C, F) during conductivity measurements.

with longer bench-top dehydration periods, but returned to zero when measured at the end of the experimental run (Figure 5).

Hydraulic VCs were constructed for both pressure heads from inlet and outlet K_h using four approaches: (i) hydraulic steady state in K_h , (ii) hydraulic steady state in Δd , (iii) deviation in RM and (iv) start value (Figure 6). Each conductivity reading was plotted against its corresponding ψ_x . Xylem water potential was calculated from the time-dependent and diameter-dependent linear relation between ψ_x at the start and end of measurements, to account for the release in xylem tension during each experimental run (Figure 5). For the 8 kPa pressure head, a distinct sigmoidal curve with a strong fit was obtained for

hydraulic steady state in K_h and Δd (Figure 6A, Table 4). The distinction between inlet and outlet-based VCs was also minimal, clearly pointing to stability. Vulnerability curves based on RM and start value had a weaker sigmoidal fit (Table 4), and the larger divergence between inlet and outlet PLC values showed that stability was not reached, and dynamic water flow conditions were still occurring in these samples, affecting the respective K_h readings (Figure 6A, Table 4). For the 8 kPa pressure head, a Weibull function could be fitted to hydraulic steady state in K_h , as this was the only scenario generating a near 0% PLC at a xylem water potential of 0 MPa (Figure 6A). Similar findings resulted from the 2 kPa pressure head measurements, with the

Table 2. Timespan to reach hydraulic steady state according to stability in hydraulic conductivity (K_h) and stability in diameter change or radial flow (Δd) for the different bench-top dehydration periods and the two pressure heads (8 and 2 kPa).

Dehydration period (h)	$t_{\Delta(\mathcal{K}_{h,in}-\mathcal{K}_{h,out})}pprox O$ (min)		$t_{\Delta d} pprox extsf{O}$ (min)	
	8 kPa	2 kPa	8 kPa	2 kPa
0	105	232	27	205
2	105	213	28	224
4	114	216	179	81
6	223	278	93	167
8	205	/	101	/
10	279	604	160	95
12	306	308	144	100
14	348	/	163	/

Timespan when inlet K_h approximately equals outlet K_h in a threshold range of $6\pm1~10^{-8}$ kg s⁻¹ m MPa⁻¹ or when the difference between both becomes minimal ($t_{\Delta(K_{h,in}-K_{h,out})}\approx 0$, min), and timespan when diameter change becomes minimal ($t_{\Delta d}\approx 0$, min) for the different bench-top dehydration periods and the two pressure heads (8 and 2 kPa).

Table 3. Evolution of maximum hydraulic conductivity at the inlet $(K_{h,max,in})$ and outlet sides $(K_{h,max,out})$ for both pressure heads (8 and 2 kPa) and for the different bench-top dehydration periods in comparison to $K_{h,max}$ of freshly cut branches (n = 5).

Dehydration period (h)	$K_{h,max,in}$ (10 ⁻⁵ kg s ⁻¹ m MPa ⁻¹)		$K_{h,max,out}$ (10 ⁻⁵ kg s ⁻¹ m MPa ⁻¹)	
	8 kPa	2 kPa	8 kPa	2 kPa
0	9.1	8.5	8.9	8.5
2	8.9	6.9	9.2	6.6
4	6.8	6.1	6.9	6.0
6	5.4	3.5	5.4	3.4
8	4.4	/	4.1	/
10	2.7	1.8	2.5	1.8
12	1.6	1.0	1.5	0.8
14	0.9	/	0.8	/
Freshly cut Av±SD	8.6 ± 1.5	8.6 ± 0.5	8.6 ± 1.5	8.0 ± 0.

Value of maximum hydraulic conductivity at inlet side ($K_{h,max,in}$ (10⁻⁵ kg s⁻¹ m MPa⁻¹)) and outlet side ($K_{h,max,out}$ (10⁻⁵ kg s⁻¹ m MPa⁻¹)) for the different bench-top dehydration periods and the two pressure heads (8 and 2 kPa) compared with $K_{h,max}$ of freshly cut branches.

goodness of sigmoidal fit more comparable between all scenarios (Figure 6B, Table 4). Due to the lower pressure head used, maximum conductivity values decreased more rapidly for similar bench-top dehydration periods, resulting in steeper increases toward 100% PLC compared to 8 kPa pressure head (Table 3). For both pressure heads, P50 values became more negative when moving from hydraulic steady state in K_h to start value (Table 5), because the time to reach stability in K_h was longest (Table 2). The P50 derived from inlet and outlet-based VCs was minimal for hydraulic steady state in K_h and Δd , compared with deviation in RM and start value (Figure 6B, Table 5).

Hydraulic VCs based on steady state in K_h and Δd for $K_{h,out}$ were also constructed against initial xylem tension, measured at the end of bench-top dehydration prior to conductivity measurements (Figure 7). In comparison with deviation in RM and start value, these VCs had a stronger sigmoidal fit for the 8 kPa pressure head (with again a Weibull fit for steady state in K_h) but were weak for the 2 kPa pressure head (Figure 7A and B, respectively, Table 4). The P_{50} was -1.01 MPa for steady state in K_h and -1.08 MPa for steady state in Δd for the 8 kPa

pressure head, whereas P_{50} was -0.74 MPa and -0.61 MPa, respectively, for the 2 kPa pressure head (Table 5).

The µCT method

X-ray computed microtomography was applied to further assess the impact of the hydraulic method on hydraulic conductivity measurements. Because K_h of flushed branches was significantly lower than initial conductivity of freshly cut branches (Figure 3), suggesting a possible flaw in the flushing procedure, μ CT images of both states were used to visualize xylem before and after flushing (Figure 8). Because all embolized vessels were completely refilled after flushing, the flushing method was judged to work properly (Figure 8B).

The effect of small pressure heads on K_h measurements was also studied using μ CT images, which showed that vessels also refilled during an experimental run (Figure 9). For the 8 kPa pressure head, 94.7% of embolized vessels of a 12-h-dehydrated branch sample were refilled (Figure 9A and B), while for the 2 kPa pressure head, 93.4% of embolized

	8	8 kPa		kPa
	RMSE K _{h,in} (-)	RMSE K _{h,out} (-)	RMSE $K_{h,in}$ (–)	RMSE K _{h,out} (-)
Adjusted ψ_{x}				
Steady state in K _h	0.019	0.019	0.745	0.774
Steady state in Δd	0.224	0.178	0.635	0.641
Deviation RM	0.610	0.472	0.851	0.842
Start value	0.993	0.537	0.668	0.877
Initial ψ_x				
Steady state in K _h	/	0.016	/	0.767
Steady state in Δd	/	0.216	/	0.735

Root mean square error (RMSE, -) derived from Weibull and sigmoidal fits of obtained hydraulic VCs from four scenarios (hydraulic steady state in conductivity (K_h)—hydraulic steady state in radial flow (Δd)—deviation in RM—start value) against adjusted and initial xylem water potential (ψ_x), for both inlet K_h and outlet K_h and the two pressure heads (8 and 2 kPa).

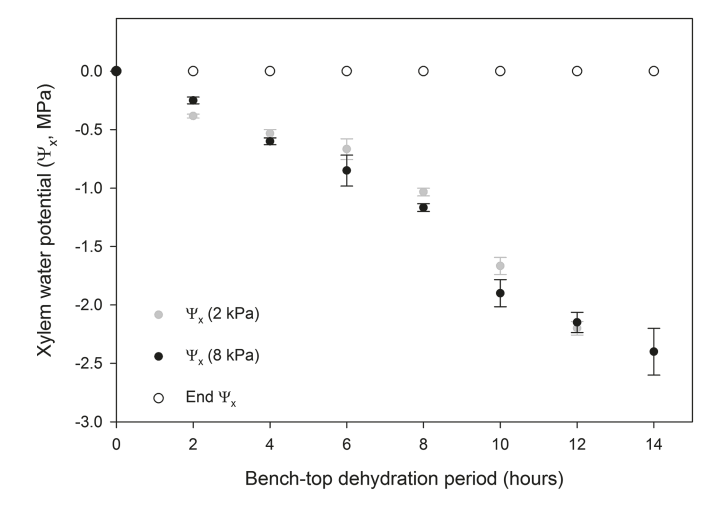


Figure 5. Average xylem water potential (ψ_x , MPa) of *M. domestica* Borkh. with standard error (1 SE) at the end of each bench-top dehydration period (h) for both the 2 kPa (light gray, closed circles) and the 8 kPa pressure head (black, closed circles). At the end of the conductivity experiment, xylem tension returned to zero independent of the bench-top dehydration period (black, open circles).

vessels of a 6-h-dehydrated branch sample were refilled (Figure 9C and D).

Acoustic emission method

The average acoustic VC, displaying changes in AE during sample dehydration continuously, resulted in a more pronounced S-shape compared with the hydraulic VC (Figure 10). The resulting AE $_{50}$ (i.e., water potential at which 50% embolism-related AE occur) was $-0.86\,\pm\,0.04$ MPa, which closely corresponded to the P $_{50}$ of -0.87 MPa derived from the 6-h-dehydrated μCT image.

Discussion

The hydraulic method has without question proven its vast reliability in quantifying hydraulic conductivity, but for determining the degree of embolism, the findings of this research clearly show that the assumption of stable conductivity is not that straightforward because of the long time required to reach steady state between inflow and outflow, influence of radial flow (Pereira and Ribeiro 2018) and possible refilling effects in embolized xylem. The approach will work for VC and P_{50} value comparisons between organs, plants and species done in the same lab using the exact same methods (e.g., Jacobsen et al. 2007, McCulloh et al. 2011), but it could prove problematic when comparison is done between different labs (e.g., Choat et al. 2012) that use different timespans, different criteria for reaching hydraulic stability and different pressure heads.

Hydraulic steady state

One of the major uncertainties when applying the hydraulic method is the timespan to reach stability, as this determines the value of $K_{h,out}$ to construct the hydraulic VC. According to Melcher et al. (2012), a deviation in RM of $K_{h,out}$, as proposed by Sperry et al. (1988a), should result in stable (steady state) measurement conditions. But measurement of water flow dynamics through the samples in the hydraulic conductivity apparatus showed that a deviation in RM did not yield stable conditions. (i) There is a distinct difference between $K_{h,in}$ and $K_{h,out}$ (on average 0.2 10^{-5} kg s⁻¹ m MPa⁻¹ for the 8 kPa pressure head, and $1.24 \times 10^{-5} \text{ kg s}^{-1} \text{ m MPa}^{-1}$ for the 2 kPa pressure head), and radial flow is rapidly increasing (on average a slope of 0.0030 mm min⁻¹ for the 8 kPa pressure head and a slope of 0.0018 mm min⁻¹ for the 2 kPa pressure head) (Figure 4). (ii) There is a distinct deviation between hydraulic VCs constructed from $K_{h,in}$ and $K_{h,out}$ (Figure 6), and between the resulting P_{50} values (Table 5). (iii) The non-steady state in hydraulic conductivity also translates in weak sigmoidal fits (Table 4). Moreover, prolonging conductivity measurements beyond a timespan of 30 min illustrates a large variability in deviation in RM making it difficult to select the value to construct the hydraulic VC, especially if only measurements of $K_{h,out}$ are considered (Figure 4).

Table 5. Derived P_{50} values from hydraulic VCs of *M. domestica* Borkh. calculated from scenarios against adjusted and initial xylem water potential, for both inlet ($K_{h,in}$) and outlet hydraulic conductivities ($K_{h,out}$) and for both pressure heads (8 and 2 kPa).

	8	8 kPa		2 kPa
	P ₅₀ K _{h,in} (MPa)	P ₅₀ K _{h,out} (MPa)	P ₅₀ K _{h,in} (MPa)	P ₅₀ K _{h,out} (MPa)
Adjusted ψ_{x}				
Steady state in K _h	-0.44	-0.44	-0.27	-0.30
Steady state in Δd	-0.59	-0.56	-0.35	-0.35
Deviation RM	-1.17	-1.09	-0.82	-0.46
Start value	-1.36	-1.20	-0.78	-0.36
Initial ψ_{x}				
Steady state in K _h	/	-1.01	/	-0.74
Steady state in Δd	/	-1.08	/	-0.61

Values of 50% loss in conductivity (P_{50} , MPa) derived from hydraulic VCs calculated from four scenarios (hydraulic steady state in conductivity (K_h)—hydraulic steady state in radial flow (Δd)—deviation in RM—start value) against adjusted and initial xylem water potential (ψ_x), for both inlet K_h and outlet K_h and the two pressure heads (8 and 2 kPa).

Based on the theory of fluid dynamics and given a constant ΔP over the measured sample, stability in hydraulic conductivity is reached at hydraulic steady state, which implies that $K_{h,in}$ must be equal to $K_{h,out}$ and radial flow zero. Only then will water move through the xylem only and will no longer be redirected to refill osmotically active living cells. Theoretically, this corresponds with stationary flow described by the Van den Honert concept (Van den Honert 1948), which is the basis for calculating xylem hydraulic conductivity (Sperry et al. 1988a). The timespan to reach hydraulic steady state increased with increased levels of dehydration (Table 2) as also observed by Hacke et al. (2015). From a physiological point of view, this pattern corresponds to water transport dynamics in intact plants and can be illustrated by the close link that exists between sap flow and stem diameter variations (Figure 11; Steppe et al. 2006, 2015). Water transport dynamics are a direct result of the time-lag that exists between foliar transpiration and root water uptake (Figure 11A and B; Schulze et al. 1985, Steppe et al. 2002). This translates into a dynamic diameter variation pattern of shrinkage (i.e., depletion of internal water reserves during the day) and swelling (i.e., replenishment of internal water reserves overnight) to overcome the imbalance between water loss and uptake (Figure 11C and D; Herzog et al. 1995, Zweifel et al. 2001, Steppe and Lemeur 2004). Measurements of stem diameter variation also provide information on radial (turgor-driven) stem increment (Steppe et al. 2006, Venturas et al. 2017), hence justifying the use of a LVDT in our study as a means to assess the impact of radial flow dynamics on K_h measurements.

Dynamic water transport in stem and branches can be described as the flow of water in two coaxial cylinders separated by a virtual membrane (Steppe et al. 2006, 2015). The first pathway is the direct flow path through the xylem driven by a water potential gradient (Van den Honert 1948), and the second one is the radial flow path, which drives changes in stem water content or hydraulic capacitance in the living tissue, also known as elastic changes. In well-watered plants,

the temporal imbalance between leaf transpiration and stem sap flow (or root water uptake) is small, and steady state or stationary flow conditions are quickly reached, with radial water flow only slightly contributing to the transpiration stream (Figure 11A). This results in a limited diameter shrinkage and swelling registered by the LVDT (Figure 11C). This explains why (i) hydraulic steady state is reached faster in samples that are less dehydrated and (ii) changes in diameter are negligible in these samples (Figure 4, Table 2). In a drought-stressed plant, the imbalance between transpiration and stem sap flow is larger, requiring a higher contribution from radial water flow to the transpiration stream. This results in a larger time-offset until equilibrium is reached (Figure 11B) and a more pronounced diameter shrinkage and swelling (Figure 11D).

Consequently, some of the observed decrease in outlet hydraulic conductivity by Wheeler et al. (2013) in branches cut under tension could be the result of the depleted internal reserves that stimulate radial flow once connected to the hydraulic conductivity apparatus instead of artificial embolism formation by the cut. Moreover, the imbalance was also witnessed in asparagus, where longer bench-top dehydration periods needed to measure the more dehydrated samples resulted in larger offsets between inlet and outlet hydraulic conductivity measurements (Figure 1; Zinkernagel and Mayer 2018), demonstrating that the dynamic water transport principles hold for both woody and herbaceous species. We can thus conclude, independently of the examined species, that the longer the bench-top dehydration period, the longer it takes to reach hydraulic steady state, and the more pronounced the increase in stem diameter will be during K_h measurements (Figure 4, Table 2).

By extending the original hydraulic conductivity apparatus with additional measurements, a solid background was provided to assess the impact of different (i.e., steady state and non-steady state) K_h values to construct hydraulic VCs. Hydraulic VCs based on steady state in K_h and Δd were more justified approaches to depict vulnerability to drought-induced embolism

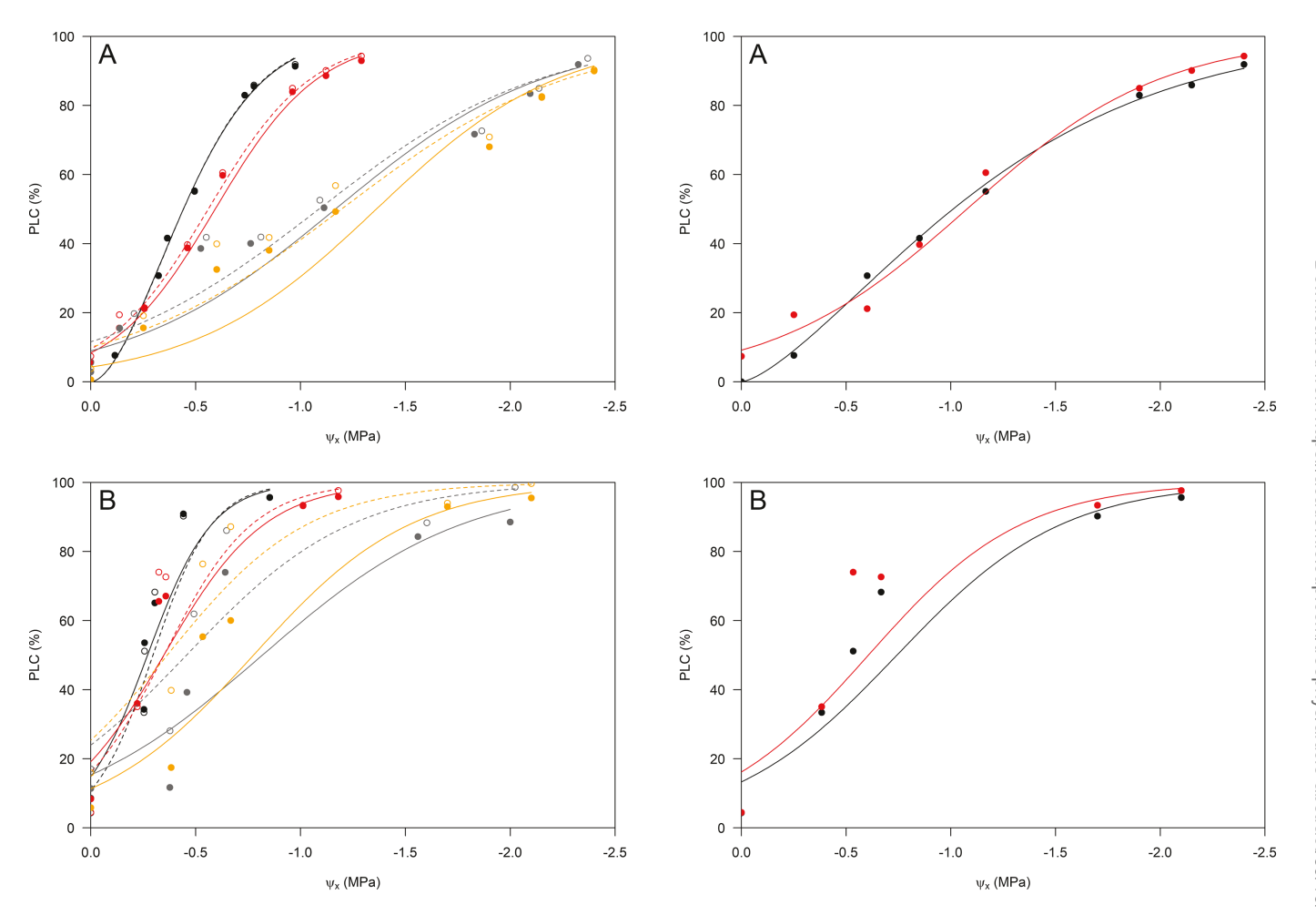


Figure 6. Hydraulic VCs of M.domestica Borkh. showing percentage loss of conductivity (PLC, %) against adjusted xylem water potential (ψ_x , MPa) derived from hydraulic steady state in hydraulic conductivity (K_h , 10^{-5} kg s⁻¹ m MPa⁻¹) for inlet hydraulic conductivity ($K_{h,in}$, black, closed circles) and outlet hydraulic conductivity ($K_{h,out}$, black, open circles), derived from hydraulic steady state in diameter change or radial flow (Δd , mm) for $K_{h,in}$ (red, closed circles) and $K_{h,out}$ (red, open circles), derived from deviation in RM for $K_{h,in}$ (light gray, closed circles) and $K_{h,out}$ (light gray, open circles), and derived from start value for $K_{h,in}$ (orange, closed circles) and $K_{h,out}$ (orange, open circles). Vulnerability curves are shown for the 8 kPa (A) and 2 kPa pressure head (B) and are fitted with a sigmoidal model with the exception of the Weibull fit for hydraulic steady state in K_h of the 8 kPa pressure head.

in M. domestica Borkh. (Figure 6). Stability was illustrated by the strong overlap between VCs based on $K_{h,in}$ and $K_{h,out}$ (Figure 6, Table 5) and could be described by a strong sigmoidal fit (Table 4). Hydraulic steady state in Δd was defined at the breakpoint distinguishing faster from slower increases in stem diameter. While this approach is easy to use, it still includes a small radial water flow effect, which explains why the timespan to reach stable Δd was shorter than for stability in K_h (Table 2). Vulnerability curves based on hydraulic steady state in K_h were the only ones providing near 0% PLC in hydrated samples, suggesting that steady state in K_h is the best proxy for overall hydraulic steady state (Figure 6).

Figure 7. Hydraulic VCs of M. domestica Borkh. showing percentage loss of conductivity (PLC, %) against initial xylem water potential (ψ_x , MPa) derived from hydraulic steady state in hydraulic conductivity (K_h , 10^{-5} kg s⁻¹ m MPa⁻¹) for outlet hydraulic conductivity ($K_{h,out}$, black), and derived from hydraulic steady state in diameter change or radial flow (Δd , mm) for $K_{h,out}$ (red). Vulnerability curves are shown for the 8 kPa (A) and 2 kPa pressure head (B) and are fitted with a sigmoidal model with the exception of the Weibull fit for hydraulic steady state in K_h of the 8 kPa pressure head.

Assessment of the hydraulic method

Being able to objectively quantify hydraulic steady-state flow conditions in the study samples addresses one of the major concerns regarding the use of the hydraulic method. By using this approach, we discovered an additional and substantial flaw in the theory behind the hydraulic method. According to Sperry et al. (1988a), low-pressure heads in the range of 1 to 8 kPa would be insufficient to refill embolized vessels (Kolb et al. 1996, Melcher et al. 2012). At first glance, this seemed to hold because the difference between $P_{\rm in}$ and $P_{\rm out}$ (i) remained constant during an experimental run and (ii) increased with the duration of bench-top dehydration, which was explained by an increased resistance in xylem flow path (Figure 4).

The dynamic change in ψ_x occurring during each experimental run required calculation of adjusted, steady-state (instead

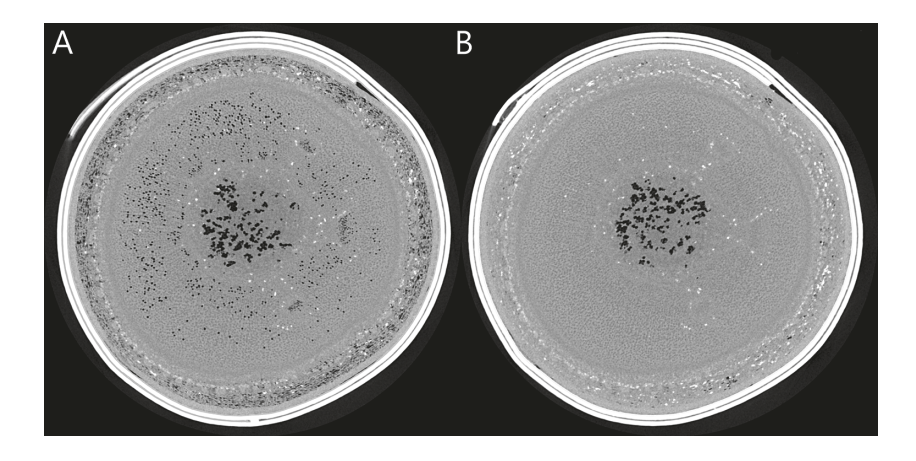


Figure 8. (A) X-ray computed microtomography image illustrating native embolism (black dots) of a freshly cut M. domestica Borkh. sample. (B) A μ CT image of a flushed M. domestica Borkh. sample, showing that the flushing method was capable of refilling all embolized vessels.

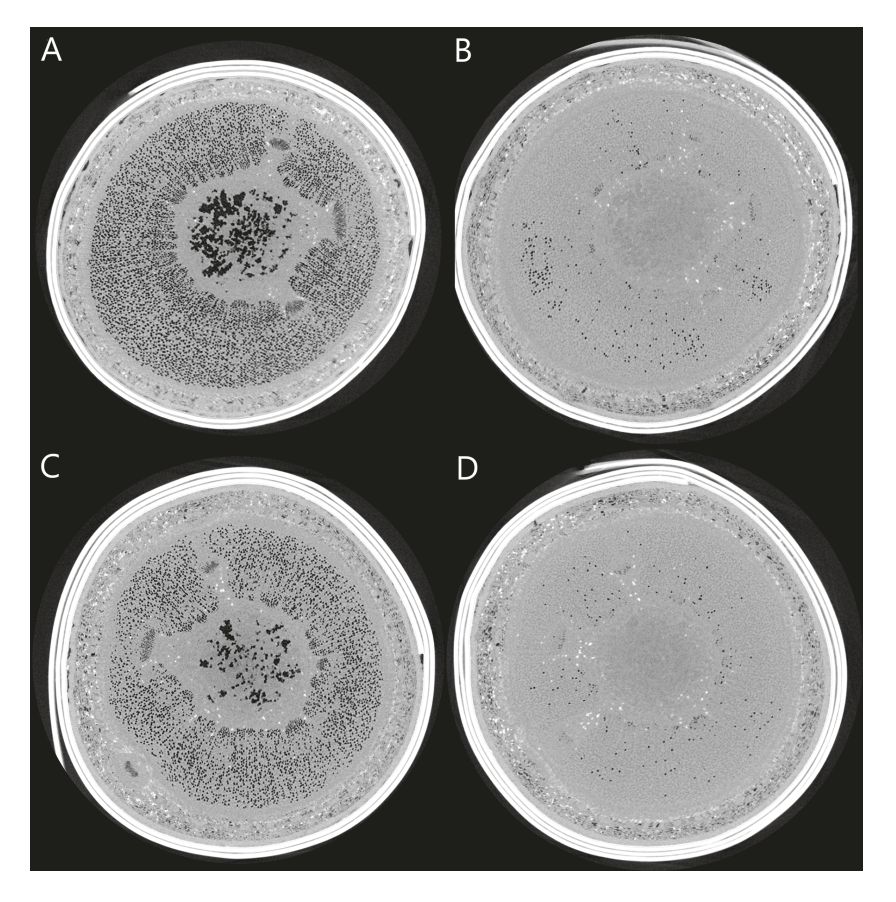


Figure 9. Montage of μ CT images illustrating the refilling of embolized vessels (black dots) of a 12-h-dehydrated M. domestica Borkh. sample under a 8 kPa pressure head (A, B) and the refilling of embolized vessels of a 6-h-dehydrated M.domestica Borkh. sample under a 2 kPa pressure head (C, D) during hydraulic conductivity measurements.

of initial) ψ_x that corresponded to the respective K_h values to construct hydraulic VCs. These hydraulic VCs strongly shifted to the left (Figure 6), with on average across the two pressure heads, a P_{50} of -0.36 MPa and -0.46 MPa, respectively (Table 5). These values are unlikely to be correct for *M. domestica* Borkh. as P_{50} values between -0.85 MPa and -3.8 MPa have previously been reported for this species (Beikircher et

al. 2013, De Baerdemaeker et al. 2018). Despite successful quantification of hydraulic steady state, the corresponding steady-state $\psi_{\rm X}$ no longer reflects the amount of embolized vessels, which were present at the end of bench-top dehydration and characterizing the intended level of drought stress. To avoid the issue of refilling, one might reason that the first measured $K_{\rm h}$ then represents actual conductivity of the drought-

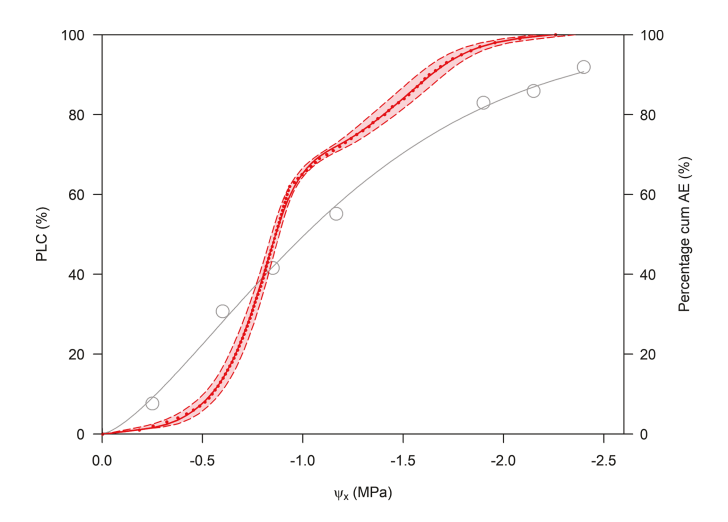


Figure 10. Hydraulic steady-state VC in outlet hydraulic conductivity ($K_{h,out}$, 10^{-5} kg s⁻¹ m MPa⁻¹) for 8 kPa pressure head (light gray, open circles), fitted with a Weibull function versus the average acoustic VC (VC_{AE}, red) with standard error bands (1 SE) of *M. domestica* Borkh. showing percentage cumulative acoustic emissions (cum AE, %) against xylem water potential (ψ_x , MPa).

stressed sample. However, constructing VCs with K_h start values showed similar issues as when deviation in RM was used: no stability, and therefore violating the steady-state precondition (Figure 6, Table 5) and a weak sigmoidal fit (Table 4). To mirror the intended drought level of the study sample, steady-state K_h and Δd values for both pressure heads were plotted against initial ψ_x (Figure 7). Resulting VCs showed a stronger sigmoidal fit, and the P_{50} values of the 8 kPa pressure head for stability in K_h and stability in Δd were well within the above-mentioned range of reported P_{50} s for this species (Table 5), but given the principles of dynamic water transport through the study samples, this approach should be used with care, because it combines steady state in K_h with initial, non-steady-state ψ_x .

These findings show that it is crucial for research using the hydraulic method to construct VCs with a uniform protocol, allowing a more correct assessment and comparison of hydraulic VCs between species and between labs. Our recommendation is to measure hydraulic conductivity in a maximum timeframe of 10 min, and at uniform timespans (e.g., after 1 min) independently of the examined species and bench-top dehydration period, and with a maximum applicable pressure head that is based on the diameter of the largest vessel (Van leperen et al. 2000). Clearly, hydraulic stability cannot be reached and is inappropriate to be used as proxy for VCrelated K_h values. Avoiding the use of very low-pressure heads is equally important, as the resulting VCs tend to be more rshaped than s-shaped (Figure 6B). The validity of r-shaped VCs has been widely debated (Jansen et al. 2015), and our findings suggest that such curves could be measurement artifacts under certain conditions.

The hydraulic method promotes embolism refilling: validation with μCT

X-ray computed microtomography allows distinguishing functional from embolized vessels without disrupting the dynamic water relations of the examined species (Cochard et al. 2015, Brodersen et al. 2018). The µCT images showed that freshly cut branches had approximately 9% native embolism (Figure 8A), and that flushing was capable of refilling all vessels (Figure 8B). By using K_h from freshly cut branches as proxy for $K_{h,max}$ to calculate PLC, the potential risk of overestimating $K_{h,max}$ by flushing vessels that lost their functionality during plant development (Jacobsen and Pratt 2012) was avoided. However, we witnessed the opposite effect, as K_h after flushing was significantly lower than initial K_h from freshly cut branches (Figure 3). Because our measurements were conducted in August and September, our Malus species was in the fruit ripening period. Knipfer et al. (2015), referring to the study of Choat et al. (2009) and that of Lang and Ryan (1994), highlighted that fleshy fruit species like apple lose a part of their transport ability during ripening. Choat et al. (2009), who examined the phenomenon on grapevine, found higher concentrations of xylem solutes in grapevine post-veraison and related this to the deposition of gels into the xylem vessel lumen. Therefore, a possible hypothesis might be that high-pressure flushes can dislocate these gels present in vessel lumens (Jacobsen and Pratt 2012), which can then clog the remaining vessels of the sample. This significant problem has been previously addressed by Espino and Schenk (2011). Another and perhaps even likely hypothesis is that embolism potentially can change pit membrane structures (S. Jansen, personal communication) and that the interaction with high-pressure flushes result in a reduction in hydraulic conductivity when measured with lowpressure heads.

Not only high-pressure flushing, but also low-positivepressure heads were capable of refilling embolized vessels, which was already shown by Knipfer et al. (2016), even though that was long assumed to not be the case (Sperry et al. 1988a). Both, 8 and 2 kPa pressure heads refilled about 94% of the cavitated vessels (Figure 9), questioning the use of pressurized water to quantify drought-induced embolism. This refilling also explains the increase in K_h (Figure 4), and in ψ_x (Figure 5) during each experimental run, which is supported by the findings of Brodersen et al. (2010) and Brodersen and McElrone (2013), who observed less negative xylem water potentials after vessels refilled. Additionally, the 12 h dehydrated sample swelled 6.6% due to refilling under 8 kPa (Figure 9A and B), and the 6-h-dehydrated sample swelled 2.4% due to refilling under 2 kPa (Figure 9C and D), emphasizing the importance of considering dynamic water flow in study samples when using the hydraulic method (Figure 4). The fact that small positive pressure heads can refill embolized vessels is not that unlikely if one considers the phenomenon

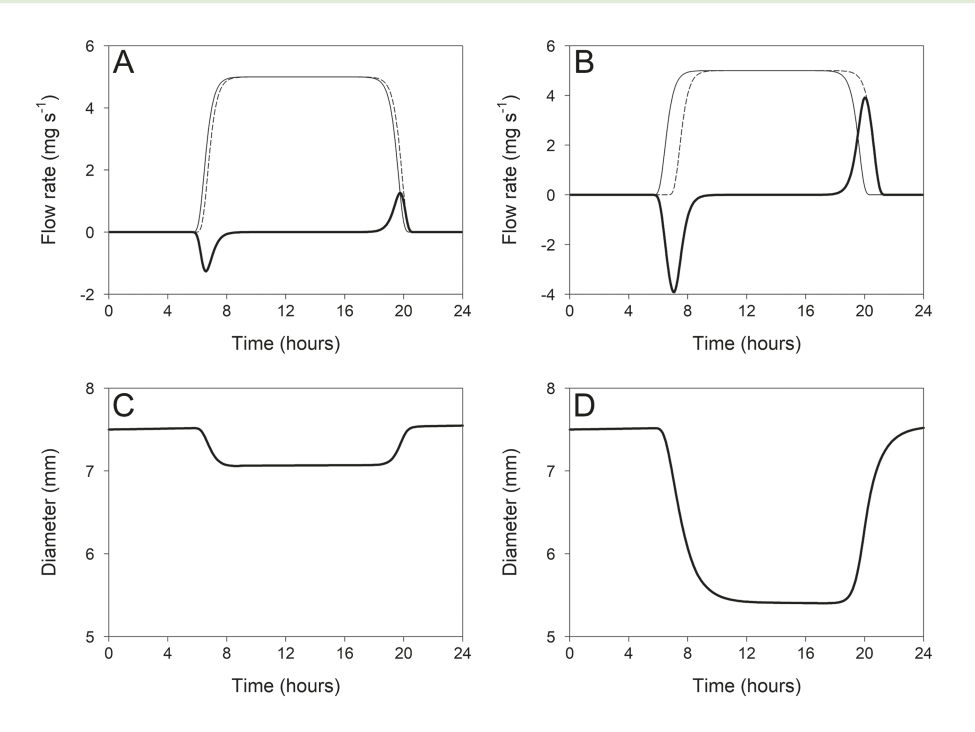


Figure 11. Synthesis of dynamic water transport showing the diurnal course of transpiration rate (solid black line), stem sap flow (dashed black line) and stem water content depletion rate (thick solid black line) for a well-watered (A) and water-stressed plant (B), and the diurnal course of diameter variation (thick black line) for a well-watered (C) and water-stressed plant (D). The tight coupling between stem flow and diameter variation illustrates that the dynamic behavior emerges from the time lag between water loss by transpiration and root water uptake. The temporal imbalance takes longer to overcome under drought stress, putting more strain on the internal water reserves.

of root pressure (Tyree and Sperry 1989a). Root pressure is a widely accepted mechanism to explain recovery from daily cycles of embolism formation in intact plants (Tyree and Zimmermann 2002). In general, root pressure is very weak with values only slightly exceeding atmospheric pressure (typical range: 1–150 kPa; see Sperry et al. 1988b, Fisher et al. 1997, De Swaef et al. 2013, Lopez and Barclay 2017). During the day, its influence is negligible, but during the night, when transpiration is zero, root pressure pushes up the sap, dissolving air bubbles and refilling embolized vessels (Tyree and Zimmermann 2002, Wegner 2014).

Hydraulic versus AE method

Quantification of vulnerability to drought-induced embolism is crucial in drought-related plant research, but the difficulty of the hydraulic method in deciding which $K_{\rm h}$ value best depicts the degree of embolism and the dynamic refilling effect of the method suggest that there is merit in other techniques that do not interfere with the hydraulic properties of the branch, such as the acoustic method (Rosner et al. 2006, Mayr and Rosner 2011, Nolf et al. 2015, Vergeynst et al. 2015a, De Baerdemaeker et al. 2017). We tested the acoustic (AE) method to determine if it could be a reliable substitute for measuring P_{50} values (Figure 10). The average AE_{50} of -0.86 MPa with a standard error of only 0.04 MPa for M. M domestica Borkh. M illustrates the consistency and accuracy of the AE method,

which can also continuously measure changes in dehydration without creating conditions for radial flow, embolism refilling and xylem tension changes (Rosner et al. 2006, Mayr and Rosner 2011, Vergeynst et al. 2015a, De Baerdemaeker et al. 2017, Pereira and Ribeiro 2018). Already in 1983, Tyree and Dixon (1983) highlighted the importance of the AE technique as a powerful diagnostic tool to describe plant water relations. The method of course cannot quantify $K_{\rm h}$, and further research is required on the origins of AE from drying plant tissues (Cochard et al. 2013), but recent and ongoing developments are promising for the use of AE as a reliable alternative to the hydraulic method to construct VCs (Wolkerstorfer et al. 2012, De Roo et al. 2016).

Conclusion

Hydraulic methods are irreplaceable for quantification of hydraulic conductivity, and have been used successfully to compare vulnerabilities to embolism between plant organs, plants and species. There is no doubt that such comparisons are meaningful when obtained using the exact same methods, but our findings show that comparisons can become problematic when VCs and P_{50} values are compared between studies that used slightly different methods and different criteria for stability in $K_{\rm h}$, because slight differences in the methodology can have large impacts on the measurements. By extending the

original hydraulic setup, fundamental insights were gathered to tackle the K_h stability enigma, as hydraulic steady state was dependent on water flow dynamics, such as radial flow, xylem tension release and refilling of embolized vessels. When publishing hydraulic results, it is important to consider that stability in K_h is not the best criterion to characterize the degree of embolism. To standardize measurements and avoid vulnerability overestimation, we recommend standardizing the protocol by taking K_h readings within a timeframe of 10 min at uniform timespans (e.g., after 1 min), as this allows insufficient time for significant radial flow, embolism refilling, and xylem tension dissipation phenomena. Methods that (i) can measure dehydration continuously on a single sample, without disrupting dynamic water relations and (ii) are practical and cost-effective can be used as reliable substitutes for the hydraulic method. The AE technique has these desirable traits and is thus a promising alternative to hydraulic methods for VC construction.

Supplementary Data

Supplementary Data for this article are available at *Tree Physiol*ogy Online.

Acknowledgments

The authors wish to thank two colleagues of the Laboratory of Plant Ecology, Ghent University: Philip Deman for the technical preparation of the experimental setup and Geert Favyts for the construction of sample holders used in the hydraulic conductivity apparatus. Sincere gratitude toward our colleague Olivier Leroux at the Department of Biology, Faculty of Sciences, Ghent University for preparing and finalizing the microscopic wood section and toward the Centre for Advanced Light Microscopy at Ghent University (Belgium) for their support and assistance on nanoparticle tracking analysis. The authors also gratefully acknowledge the work of the handling Editor and anonymous reviewers in evaluating and improving our manuscript.

Conflict of interest

None declared.

Funding

This work was supported by the National Science Foundation (grant no. IOS-1146993 to H.J.S., K.S. and S.J.) and the Research Foundation Flanders (FWO) (grant no. G.0319.13N and G.0941.15N to K.S. supporting the PhD of N.J.F.D.B.).

References

Alder NN, Pockman WT, Sperry JS, Nuismer SM (1997) Use of centrifugal force in the study of xylem cavitation. J Exp Bot 48:665–674.

- Allen CD, Macalady AK, Chenchouni H et al. (2010) A global overview of drought heat-induced tree mortality reveals emerging climate change risks for forests. For Ecol Manage 259:660-684.
- Balaz M, Jupa R, Jansen S, Cobb A, Gloser V (2016) Partitioning of vessel resistivity in three liana species. Tree Physiol 33: 1296-1307.
- Beikircher B, De Cesare C, Mayr S (2013) Hydraulics of high-yield orchard trees: a case study of three Malus domestica cultivars. Tree Physiol 33:1296-1307.
- Brodersen CR, McElrone AJ (2013) Maintenance of xylem network transport capacity: a review of embolism repair in vascular plants. Front Plant Sci 4:108.
- Brodersen CR, McElrone AJ, Choat B, Matthews M, Shackel K (2010) The dynamics of embolism repair in xylem: in vivo visualizations using high-resolution computed tomography. Plant Physiol 154:1088-1095.
- Brodersen CR, Knipfer T, McElrone AJ (2018) In vivo visualization of the final stages of xylem vessel refilling in grapevine (Vitis vinifera) stems. New Phytol 217:117-126.
- Brodribb TJ (2009) Xylem hydraulic physiology: the functional backbone of terrestrial plant productivity. Plant Sci 177:245-251.
- Brodribb TJ, Bowman DJ, Nichols S, Delzon S, Burlett R (2010) Xylem function and growth rate interact to determine recovery rates after exposure to extreme water deficit. New Phytol 188: 533-542.
- Choat B, Gambetta GA, Schackel KA, Matthews MA (2009) Vascular function in grape berries across development and its relevance to apparent hydraulic isolation. Plant Physiol 151:1677-1687.
- Choat B, Drayton WM, Brodersen C, Matthews MA, Shackel KA, Wada H, McElrone AJ (2010) Measurement of vulnerability to water stress-induced cavitation in grapevine: a comparison of four techniques applied to a long-vesseled species. Plant Cell Environ 33:1502–1512.
- Choat B, Jansen S, Brodribb TJ et al. (2012) Global convergence in the vulnerability of forests to drought. Nature 491:752–755.
- Christensen-Dalsgaard KK, Tyree MT, Mussone PG (2011) Surface tension phenomena in the xylem sap of three diffuse porous temperate tree species. Tree Physiol 31:361-368.
- Cochard H (2006) Cavitation in trees. CR Phys 7:1018-1026.
- Cochard H, Bodet C, Améglio T, Cruiziat P (2000) Cryo-scanning electron microscopy observations in walnut petioles. Facts or artifacts? Plant Physiol 124:1191-1202.
- Cochard H, Badel E, Herbette S, Delzon S, Choat B, Jansen S (2013) Methods for measuring plant vulnerability to cavitation: a critical review. J Exp Bot 64:4779-4791.
- Cochard H, Delzon S, Badel E (2015) X-ray microtomography (micro-CT): a reference technology for high-resolution quantification of xylem embolism trees. Plant Cell Environ 38: 201-206.
- De Baerdemaeker NJF, Salomón RL, De Roo L, Steppe K (2017) Sugars from woody tissue photosynthesis reduce xylem vulnerability to cavitation. New Phytol 216:720-727.
- De Baerdemaeker NJF, Hias N, Van Den Bulcke J, Keulemans W, Steppe K (2018) The effect of polyploidization on tree hydraulic functioning. Am J Bot 105:161–171.
- De Roo L, Vergeynst LL, De Baerdemaeker NJF, Steppe K (2016) Acoustic emissions to measure drought-induced cavitation in plants. Appl Sci 6:71.
- De Swaef T, Hanssens J, Cornelis A, Steppe K (2013) Nondestructive estimation of root pressure using sap flow, stem diameter measurements and mechanistic modelling. Ann Bot 111:
- Dierick M, Masschaele B, Van Hoorebeke L (2004) Octopus, a fast and user-friendly tomographic reconstruction package developed in LabView (R). Meas Sci Technol 15:1366-1370.

- Dierick M, Van Loo D, Masschaele B, Van Den Bulcke J, Van Acker J, Cnudde V, Van Hoorebeke L (2014) Recent micro-CT scanner developments at UGCT. Nucl Instrum Meth B 324:35–40.
- Dixon HH, Joly J (1895) On the ascent of sap. Philos T R Soc Lond 186:563-576.
- Duursma RA, Choat B (2017) Fitplc—an R package to fit hydraulic vulnerability curves. J Plant Hydr 4:e-002.
- Epila J, De Baerdemaeker NJF, Vergeynst LL, Maes WH, Beeckman H, Steppe K (2017) Capacitive water release and internal leaf water relocation delay drought-induced cavitation in African Maesopsis eminii. Tree Physiol 37:481–490.
- Espino S, Schenk HJ (2011) Mind the bubbles: achieving stable measurements of maximum hydraulic conductivity through woody plant samples. J Exp Bot 62:1119–1132.
- Ewers FW, Fisher JB (1989) Techniques for measuring vessel lengths and diameters in stems of woody plants. Am J Bot 76: 645–656.
- Fisher JB, Guillermo AA, Ewers FW, López-Portillo J (1997) Survey of root pressure in tropical vines and woody species. Int J Plant Sci 158:44–50.
- Hacke UG, Sperry JS, Pittermann J (2000) Limits to xylem refilling under negative pressure in Laurus nobilis and Acer negundo. Plant Cell Environ 26:303–311.
- Hacke UG, Sperry JS (2003) Cavitation fatigue. Embolism and refilling cycles can weaken the cavitation resistance of xylem. Plant Physiol 125:779–786.
- Hacke UG, Venturas MD, Mackinnon ED, Jacobsen AL, Sperry JS, Pratt RB (2015) The standard centrifuge method accurately measures vulnerability curves of long-vesselled olive stems. New Phytol 205:116–127.
- Herzog KM, Häsler R, Thum R (1995) Diurnal changes in the radius of a subalpine Norway spruce stem: their relation to the sap flow and their use to estimate transpiration. Trees 10:94–101.
- Hölttä T, Cochard H, Nikinmaa E, Mencuccini M (2009) Capacitive effect of cavitation in xylem conduits: results from a dynamic model. Plant Cell Environ 32:10–21.
- Hubeau M, Steppe K (2015) Plant-PET scans: in vivo mapping of xylem and phloem functioning. Trends Plant Sci 20:676–685.
- Jacobsen AL, Pratt RB (2012) No evidence for an open vessel effect in centrifuge-based vulnerability curves of a long-vesselled liana (*Vitis vinifera*). New Phytol 194:982–990.
- Jacobsen AL, Ewers FW, Pratt RB, Paddock WA III, Davis SD (2005) Do xylem fibres affect vessel cavitation resistance? Plant Physiol 139:546–556.
- Jacobsen AL, Pratt RB, Davis SD, Ewers FW (2007) Cavitation resistance and seasonal hydraulics differ among three arid Californian plant communities. Plant Cell Environ 30:1599–1609.
- Jacobsen AL, Tobin MF, Toschi HS, Percolla MI, Pratt RB (2016) Structural determinants of increased susceptibility to dehydrationinduced cavitation in post-fire resprouting chaparral shrubs. Plant Cell Environ 39:2473–2485.
- Jansen S, Schuldt B, Choat B (2015) Current controversies and challenges in applying plant hydraulic techniques. New Phytol 205:961–964.
- Kim HK, Park J, Hwang I (2014) Investigating water transport through the xylem network in vascular plants. J Exp Bot 65: 1895–1904.
- Knipfer T, Fei J, Gambetta GA, McElrone AJ, Schackel KA, Matthews MA (2015) Water transport properties of the grape pedicel during fruit development: insights into xylem anatomy and function using microtomography. Plant Physiol 168:1590–1602.
- Knipfer T, Cuneo IF, Brodersen CR, McElrone AJ (2016) In situ visualization of the dynamics in xylem embolism formation and removal

- in the absence of root pressure: a study on excised grapevine stems. Plant Physiol 171:1024–1036.
- Kolb KJ, Sperry JS, Lamont BB (1996) A method for measuring xylem hydraulic conductance and embolism in entire root and shoot systems. J Exp Bot 47:1805–1810.
- Lang A, Ryan KG (1994) Vascular development and sap flow in apple pedicels. Ann Bot 74:381–388.
- Li Y, Sperry JS, Taneda H, Bush SE, Hacke UG (2008) Evaluation of centrifugal methods for measuring xylem cavitation in conifers, diffuse- and ring-porous angiosperms. New Phytol 177:558–568.
- Lopez FB, Barclay GF (2017) Chapter 4—Plant anatomy and physiology. In: Badal S, Delgoda R (eds) Pharmacognosy. Academic Press, Boston, MA, pp 45–60.
- Martinez-Vilalta J, Prat E, Oliveras I, Piñol J (2002) Xylem hydraulic properties of roots and stems of nine Mediterranean woody species. Oecologia 133:19–29.
- Martin-StPaul NK, Longepierre D, Huc R, Delzon S, Burlett R, Joffre R, Rambal S, Cochard H (2014) How reliable are methods to assess xylem vulnerability to cavitation? The issue of 'open vessel' artefact in oaks. Tree Physiol 34:894–905.
- Mayr S, Rosner S (2011) Cavitation in dehydrating xylem of *Picea abies*: energy properties of ultrasonic emissions reflect tracheid dimensions. Tree Physiol 31:59–67.
- Mayr S, Kartusch B, Kikuta S (2014) Evidence for air-seeding: watching the formation of embolism in conifer xylem. J Plant Hydraul 1:e0004.
- McCulloh KA, Meinzer FC, Sperry JS, Lachenbruch B, Voelker SL, Woodruff DR, Domec JC (2011) Comparative hydraulic architecture of tropical tree species representing a range of successional stages and wood density. Oecologia 167:27–37.
- Melcher PJ, Holbrook M, Burns MJ, Zwieniecki MA, Cobb AR, Brodribb TJ, Choat B, Sack L (2012) Measurements of stem xylem hydraulic conductivity in the laboratory and field. Methods Ecol Evol 3:685–694.
- $\label{eq:MuggeoVMR} \mbox{Muggeo VMR (2008) Segmented: an R package to fit regression models broken-line relationships. R News 8:20–25.}$
- Nardini A, Dimasi F, Klepsch M, Jansen S (2012) Ion-mediated enhancement of xylem hydraulic conductivity in four *Acer* species: relationships with ecological and anatomical features. Tree Physiol 32:1434–1441.
- Nolf M, Beikircher B, Rosner S, Nolf A, Mayr S (2015) Xylem cavitation resistance can be estimated based on time-dependent rate of acoustic emissions. New Phytol 208:625–632.
- Ogle K, Barber JJ, Willson C, Thompson B (2009) Hierarchical statistical modeling of xylem vulnerability to cavitation. New Phytol 182:541–554.
- Pammenter NW, Van der Willigen CV (1998) A mathematical and statistical analysis of the curves illustrating vulnerability of xylem to cavitation. Tree Physiol 18:589–593.
- Pereira L, Ribeiro RV (2018) Radial stem flow and its importance when measuring xylem hydraulic conductance. Theor Exp Plant Physiol 30:71–75.
- Pfautsch S, Renard J, Tjoelker MG, Salih A (2015a) Phloem as capacitor: radial transfer of water into xylem of tree stems occurs via symplastic transport in ray parenchyma. Plant Physiol 167:963–971.
- Pfautsch S, Hölttä T, Mencuccini M (2015b) Hydraulic functioning of tree stems—fusing ray anatomy, radial transfer and capacitance. Tree Physiol 35:706–722.
- Rosner S, Klein A, Wimmer R, Karlsson B (2006) Extraction of features from ultrasound acoustic emissions: a tool to assess the hydraulic vulnerability of Norway spruce trunkwood? New Phytol 171: 105–116.
- Ryan MG, Phillips N, Bond BJ (2006) The hydraulic limitation hypothesis revisited. Plant Cell Environ 29:367–381.

- Sala A, Woodruff DR, Meinzer FC (2012) Carbon dynamics in trees: feast or famine? Tree Physiol 32:764–775.
- Sano Y, Okamura Y, Utsumi Y (2005) Visualizing water-conducting pathways of living trees: selection of dyes and tissue preparation methods. Tree Physiol 25:269–275.
- Schenk JH, Steppe K, Jansen S (2015) Nanobubbles: a new paradigm for air-seeding in xylem. Trends Plant Sci 20:199–205.
- Schenk JH, Espino S, Rich-Cavazos SM, Jansen S (2018) From the sap's perspective: The nature of vessel surfaces in angiosperm xylem. Am J Bot 105:172–185.
- Schindelin J, Arganda-Carreras I, Frise E et al. (2012) Fiji: an open-source platform for biological-image analysis. Nat Methods 9:676–682.
- Scholander PF, Hammel HT, Bradstreet ED, Hemmingsen EA (1965) Sap pressure in vascular plants. Science 148:339–346.
- Scholz FG, Phillips NG, Bucci SJ, Meinzer FC, Goldstein G (2011) Hydraulic capacitance: biophysics and functional significance of internal water sources in relation to tree size. In: Meinzer FC, Lachenbruch B, Dawson TE (eds) Size- and age-related changes in tree structure and function. Springer, New York, NY, pp 341–362.
- Schulze ED, Cermak J, Matyssek R, Penka M, Zimmermann R, Vasicek F, Gries W, Kucera J (1985) Canopy transpiration and water fluxes in the xylem of the trunk of *Larix* and *Picea* trees—a comparison of xylem flow, porometer and cuvette measurements. Oecologia 66: 475–483.
- Sperry JS, Donnelly JR, Tyree MT (1988a) A method for measuring hydraulic conductivity and embolism in xylem. Plant Cell Environ 11:35–40.
- Sperry JS, Donnelly JR, Tyree MT (1988b) Seasonal occurrence of xylem embolism in sugar maple (*Acer saccharum*). Am J Bot 75:1212–1218.
- Sperry JS, Tyree MT, Donnelly JR (1988c) Vulnerability of xylem to embolism in a mangrove vs an inland species of Rhizophoraceae. Physiol Plant 74:276–283.
- Steppe K (2018) The potential of the water potential. Tree Physiol 38:937–940.
- Steppe K, Lemeur R (2004) An experimental system for analysis of the dynamic sap-flow characteristics in young trees: results of a beech tree. Funct Plant Biol 31:83–92.
- Steppe K, Lemeur R, Samson R (2002) Sap flow dynamics of a beech tree during the solar eclipse of 11 august 1999. Agric For Meteorol 112:139–149.
- Steppe K, De Pauw DJW, Lemeur R, Vanrolleghem PA (2006) A mathematical model linking tree sap flow dynamics to daily stem diameter fluctuations and radial stem growth. Tree Physiol 26: 257–273.
- Steppe K, Sterck F, Deslauriers A (2015) Diel growth dynamics in tree stems: linking anatomy and ecophysiology. Trends Plant Sci 20:335–343.
- Steudle E (2001) The cohesion-tension mechanism and the acquisition of water by plants root. Annu Rev Plant Phys 52:847–875.
- Torres-Ruiz JM, Sperry JS, Fernández JE (2012) Improving xylem hydraulic conductivity measurements by correcting the error caused by passive water uptake. Physiol Plant 146:129–135.
- Torres-Ruiz JM, Jansen S, Choat B et al. (2015) Direct X-ray microtomography observation confirms the induction of embolism upon xylem cutting under tension. Plant Physiol 167:40–43.
- Trifilò P, Raimondo F, Lo Gullo MA, Barbera PM, Salleo S, Nardini A (2014) Relax and refill: xylem hydration prior to hydraulic measurements favours embolism repair in stems and generates artificially low PLC values. Plant Cell Environ 37:2491–2499.
- Tyree MT, Dixon MA (1983) Cavitation events in *Thuja occidentalis* L.? Ultrasonic acoustic emissions from the sapwood can be measured. Plant Physiol 72:1094–1099.

- Tyree MT, Ewers FW (1991) The hydraulic architecture of trees and other woody plants. New Phytol 119:345–360.
- Tyree MT, Sperry JS (1989a) Vulnerability of xylem to cavitation and embolism. Annu Rev Plant Biol 40:19–36.
- Tyree MT, Sperry JS (1989b) Characterization and propagation of acoustic emission signals in woody plants: towards an improved acoustic emission counter. Plant Cell Environ 40:19–38.
- Tyree MT, Yang SD (1990) Water-storage capacity of *Thuja*, *Tsuga* and *Acer* stems measured by dehydration isotherms—the contribution of capillary water and cavitation. Planta 182:420–426.
- Tyree MT, Zimmermann MH (2002) Xylem structure and the ascent of sap, 2nd edn. Springer-Verlag, Berlin.
- Van Bel AJE (2003) The phloem, a miracle of ingenuity. Plant Cell Environ 26:125–149.
- Van den Honert TH (1948) Water transport in plants as a catenary process. Discuss Faraday Soc 3:146–153.
- Van leperen W, Van Meeteren U, Van Gelder H (2000) Fluid ionic composition influences hydraulic conductance of xylem conduits. J Exp Bot 51:769–776.
- Venturas MD, MacKinnon MD, Dario HL, Jacobsen AL, Pratt RB, Davis SD (2016) Chaparral shrub hydraulic traits, size, and life history types relate to species mortality during California's historic drought of 2014. PLoS ONE 11:e0159145.
- Venturas MD, Sperry JS, Hacke UG (2017) Plant xylem hydraulics: what we understand, current research, and future challenges. J Integr Plant Biol 59:356–389.
- Vergeynst LL, Dierick M, Bogaerts J, Cnudde V, Steppe K (2015a) Cavitation: a blessing in disguise? New method to establish vulnerability curves and assess hydraulic capacitance of woody tissues. Tree Physiol 35:400–409.
- Vergeynst LL, Sause MGR, Hamstad MA, Steppe K (2015b) Deciphering acoustic emission signals in drought stressed branches: the missing link between source and sensor. Front Plant Sci 6:494.
- Vergeynst LL, Sause MGR, De Baerdemaeker NJF, De Roo L, Steppe K (2016) Clustering reveals cavitation-related acoustic emission signals from dehydrating branches. Tree Physiol 36:786–796.
- Vlassenbroeck J, Dierick M, Masschaele B, Cnudde V, Van Hoorebeke L, Jacobs P (2007) Software tools for quantification of Xray microtomography at the UGCT. Nucl Instrum Meth A 580: 442–445.
- Wegner LH (2014) Root pressure and beyond: energetically uphill water transport into xylem vessels? J Exp Bot 65:381–393.
- Wheeler JK, Huggett BA, Tofte AN, Rockwell FE, Holbrook NM (2013) Cutting xylem under tension or supersaturated with gas can generate PLC and the appearance of rapid recovery from embolism. Plant Cell Environ 36:1938–1949.
- Wolkerstorfer SV, Rosner S, Hietz P (2012) An improved method and data analysis for ultrasound acoustic emissions and xylem vulnerability in conifer wood. Physiol Plant 146:184–191.
- Zimmermann MH, Jeje AA (1981) Vessel-length distribution in stems of some American woody plants. Can J Bot 59: 1882–1892.
- Zimmermann MH (1983) Xylem structure ant the ascent of sap. Springer-Verlag, Berlin.
- Zinkernagel J, Mayer N (2018) Water absorption into stems affects the measurement of vulnerability curves as a function of plant water status. Acta Hortic 1222:21–26.
- Zinkernagel J, Mayer N, Paschold P-J (2011) Methodological approach for identifying changes in xylem vulnerability of *Asparagus officinalis* L. during the vegetation period. Eur J Hortic Sci 76: 136–141.
- Zweifel R, Item H, Häsler R (2001) Link between diurnal stem radius changes and tree water relations. Tree Physiol 21:869–877.